ER membrane–bending proteins are necessary for de novo nuclear pore formation

T. Renee Dawson,[1] Michelle D. Lazarus,[1] Martin W. Hetzer,[2] and Susan R. Wente[1]

[1]Department of Cell and Developmental Biology, Vanderbilt University Medical Center, Nashville, TN 37232
[2]Molecular and Cell Biology Laboratory, Salk Institute for Biological Studies, La Jolla, CA 92037

Nucleocytoplasmic transport occurs exclusively through nuclear pore complexes (NPCs) embedded in pores formed by inner and outer nuclear membrane fusion. The mechanism for de novo pore and NPC biogenesis remains unclear. Reticulons (RTNs) and Yop1/DP1 are conserved membrane protein families required to form and maintain the tubular endoplasmic reticulum (ER) and the postmitotic nuclear envelope. In this study, we report that members of the RTN and Yop1/DP1 families are required for nuclear pore formation. Analysis of *Saccharomyces cerevisiae prp20-G282S* and *nup133Δ* NPC assembly mutants revealed perturbations in Rtn1–green fluorescent protein (GFP) and Yop1-GFP ER distribution and colocalization to NPC clusters. Combined deletion of *RTN1* and *YOP1* resulted in NPC clustering, nuclear import defects, and synthetic lethality with the additional absence of Pom34, Pom152, and Nup84 subcomplex members. We tested for a direct role in NPC biogenesis using *Xenopus laevis* in vitro assays and found that anti-Rtn4a antibodies specifically inhibited de novo nuclear pore formation. We hypothesize that these ER membrane–bending proteins mediate early NPC assembly steps.

Introduction

The pores formed by fusion of the inner and outer membranes of the nuclear envelope (NE) provide the passageways for all macromolecular nucleocytoplasmic exchange. Proper nuclear pore biogenesis is essential to metabolic response, cell division, and differentiation (Terry et al., 2007). Within the pore, an assemblage of ∼30 individual protein components, including nucleoporins (Nups) and three integral pore membrane proteins (Poms), comprises the framework of the nuclear pore complex (NPC): a symmetrical eightfold rotational central core with protruding cytoplasmic fibrils and a filamentous nuclear basket (Alber et al., 2007b; Lim et al., 2008). The NPC structure, of 40 MD in budding yeast and 60 MD in vertebrates, is highly modular with discrete Nup subcomplexes in distinct substructural locations (Alber et al., 2007b). This structural and compositional information has allowed many insights into the NPC assembly mechanism (for reviews see Hetzer et al., 2005; Antonin et al., 2008), yet questions remain regarding how the nuclear pore itself is formed.

Correspondence to Susan R. Wente: susan.wente@vanderbilt.edu

Abbreviations used in this paper: 5-FOA, 5-fluoroorotic acid; COP, coatomer protein; HSM, high-speed membrane; INM, inner nuclear membrane; Kap, karyopherin; NE, nuclear envelope; NPC, nuclear pore complex; Nup, nucleoporin; ONM, outer nuclear membrane; Pom, pore membrane protein; RTN, reticulon.

Two fundamental modes for NPC biogenesis exist in higher eukaryotic cells: postmitotic and de novo interphase assembly. Metazoan cells undergo an open mitosis in which the NE breaks down and NPCs disassemble into discrete subcomplexes (for review see Antonin et al., 2008). After chromatid segregation, the NE reforms via chromatin-mediated recruitment and reorganization of the tubular ER (Anderson and Hetzer, 2007, 2008), and NPCs reassemble via stepwise recruitment of Nup subcomplexes (Dultz et al., 2008). NPC assembly also must occur during interphase when the NE is intact, with a doubling of the NPC number required before the next cell division (Maul et al., 1971). These NPCs arise by de novo insertion into the NE and not by the duplication and division of existing NPCs (D'Angelo et al., 2006). Assembly into an intact NE is also required for all NPC biogenesis in organisms undergoing a closed mitosis such as the budding yeast *Saccharomyces cerevisiae* (Winey et al., 1997), suggesting that common mechanisms exist for higher and lower eukaryotes. Indeed, several critical aspects of the postmitotic and de novo NPC assembly processes are shared, with roles defined in each for the RanGTPase cycle

The Rockefeller University Press $30.00
J. Cell Biol. Vol. 184 No. 5 659–675
www.jcb.org/cgi/doi/10.1083/jcb.200806174

(Ryan et al., 2003; Walther et al., 2003b; D'Angelo et al., 2006), the transport receptor yeast (y) karyopherin 95 (Kap95)/vertebrate (v) importin-β (Harel et al., 2003a; Walther et al., 2003b; Ryan et al., 2007; D'Angelo et al., 2006), the yNup84/vNup107–160 complex (Siniossoglou et al., 1996; Harel et al., 2003b; Walther et al., 2003a; D'Angelo et al., 2006), and the Poms (Aitchison et al., 1995; Lau et al., 2004; Antonin et al., 2005; Madrid et al., 2006; Mansfeld et al., 2006; Miao et al., 2006; Stavru et al., 2006). Despite this insight into the progression of de novo NPC assembly, the precise mechanisms are not defined for triggering initial fusion of the inner nuclear membrane (INM) and outer nuclear membrane (ONM) and facilitating pore formation.

Fusion of the INM and ONM requires disruption of the lumenal leaflets, subsequent bilayer resolution to join the membranes, and stabilization of the nascent, highly curved pore. Integral membrane proteins are predicted to play key roles in membrane fusion by mediating close apposition of the INM and ONM (for review see Antonin et al., 2008). Only three integral membrane proteins are reported as being stably associated with NPCs: Pom152, Pom34, and Ndc1 in budding yeast (Wozniak et al., 1994; Chial et al., 1998; Rout et al., 2000) and gp210, Pom121, and Ndc1 in vertebrates (Greber et al., 1990; Hallberg et al., 1993; Mansfeld et al., 2006; Stavru et al., 2006). Yeast genetic studies indicate overlapping nonessential functions for Pom152 and Pom34, including interactions with specific Nups that form the NPC structural core (Madrid et al., 2006; Miao et al., 2006). Conversely, yeast Ndc1 is essential for cell viability with critical roles at both the NPC and spindle pole body (Lau et al., 2004) and is required for pore formation during postmitotic NPC assembly (Mansfeld et al., 2006; Stavru et al., 2006). However, none of these respective Poms alone are known to be sufficient for pore formation.

Recent studies have suggested a role for the yNup84/vNup107–160 complex in forming a membrane coat on the pore (Devos et al., 2004; Drin et al., 2007; Hsia et al., 2007). Nups in these complexes have α-solenoid or β-propeller domains characteristic of vesicular coating complex proteins (Siniossoglou et al., 1996; Berke et al., 2004; Devos et al., 2004; Mans et al., 2004; Alber et al., 2007b; Hsia et al., 2007). Such a coat would both stabilize the highly curved pore membranes and serve as a scaffold to incorporate additional Nups. Vesicular coat proteins are recruited to sites of vesicle budding via interactions with transmembrane proteins (Stagg et al., 2007), and, thus, interactions between the Poms and the yNup84/vNup107–160 complex might be required. Several studies have also linked non-NPC ER/NE proteins to NPC structure, function, and distribution, including ySnl1, yAcc1, yEsc1, yApq12, and vSun1 (Schneiter et al., 1996; Ho et al., 1998; Lewis et al., 2007; Liu et al., 2007; Scarcelli et al., 2007). Therefore, we speculated that additional membrane proteins of the ER and/or NE might be involved in nuclear pore formation.

Two ubiquitous ER membrane protein families have recently been linked to formation and maintenance of the highly curved tubular ER (De Craene et al., 2006; Voeltz et al., 2006; Hu et al., 2008). This includes members of the reticulon (RTN) family, with four related metazoan members (Rtn1–4 and alternatively spliced versions) and two *S. cerevisiae* members (Rtn1 and Rtn2), and a family based on the metazoan DP1 and *S. cerevisiae* Yop1. The RTN and Yop1/DP1 families do not share direct sequence homology; however, both are characterized by an ∼200–amino acid C-terminal region termed the RTN homology domain (Oertle et al., 2003). According to sequence prediction and domain mapping, the RTN homology domain forms a wedge-shaped hairpin that inserts into the outer leaflet of the lipid bilayer and contorts the ER membrane for tubule stabilization (Voeltz et al., 2006; Hu et al., 2008; Shibata et al., 2008). Moreover, recent studies have shown that metazoan RTNs and DP1 are required for proper postmitotic NE formation and growth (Kiseleva et al., 2007; Anderson and Hetzer, 2008).

In this study, we used a genetic strategy in *S. cerevisiae* to directly test Rtn1 and Yop1 for roles in NPC structure, function, and assembly. Surprisingly, Rtn1-GFP and Yop1-GFP mislocalized in the *prp20-G282S* and the *nup133Δ* nuclear pore assembly mutants. Furthermore, the *rtn1Δ yop1Δ* double mutant showed NPC structure and clustering defects and functional links to nuclear pore biogenesis. Using novel *Xenopus laevis* in vitro assays, anti-Rtn4a antibodies inhibited de novo NPC assembly and pore formation. We propose that RTNs and/or Yop1/DP1 is required to stabilize nascent pore membrane curvature during NPC biogenesis.

Results

Identification of Rtn1 and Yop1 as candidate NPC assembly factors

To assay for functional links between ER/NE proteins and NPC assembly, we used a genetic-based assay in *S. cerevisiae*. We previously characterized a novel *prp20-G282S* mutant that is defective for Ran–guanine nucleotide exchange factor function and the RanGTPase cycle (Ryan et al., 2003). The *prp20-G282S* allele specifically blocks NPC assembly into intact NEs, with fewer intact NPCs in the NE and Nup accumulation in cytoplasmic membranes (Ryan et al., 2003). We speculated that factors required for NPC assembly would have altered localization in the *prp20-G282S* mutant at the nonpermissive growth temperature (34°C). Given the recent reports of RTN and Yop1/DP1 function in stabilizing highly curved ER tubules (De Craene et al., 2006; Voeltz et al., 2006; Hu et al., 2008; Shibata et al., 2008) and in mediating metazoan postmitotic NE formation (Anderson and Hetzer, 2007, 2008; Kiseleva et al., 2007), we considered these prime candidates. We selected yeast Rtn1 and Yop1 for testing, as previous studies have documented their predominant expression and function over yeast Rtn2 (De Craene et al., 2006; Voeltz et al., 2006).

To test Rtn1 and Yop1, we generated *prp20-G282S* strains with a respective *rtn1-GFP* or *yop1-GFP* allele for analysis by confocal microscopy. The GFP-tagged protein localization was compared with the overall ER/NE structure by incorporating dsRed-HDEL (an ER/NE lumenal marker; Bevis et al., 2002). As shown in Fig. 1 A, at the permissive growth temperature (23°C), the Rtn1-GFP signal was predominantly detected at the peripheral ER near the plasma membrane with less localization at the NE. This was reflected by the overlap with the dsRed-HDEL signal (Fig. 1 A) and is consistent with previous studies for Rtn1

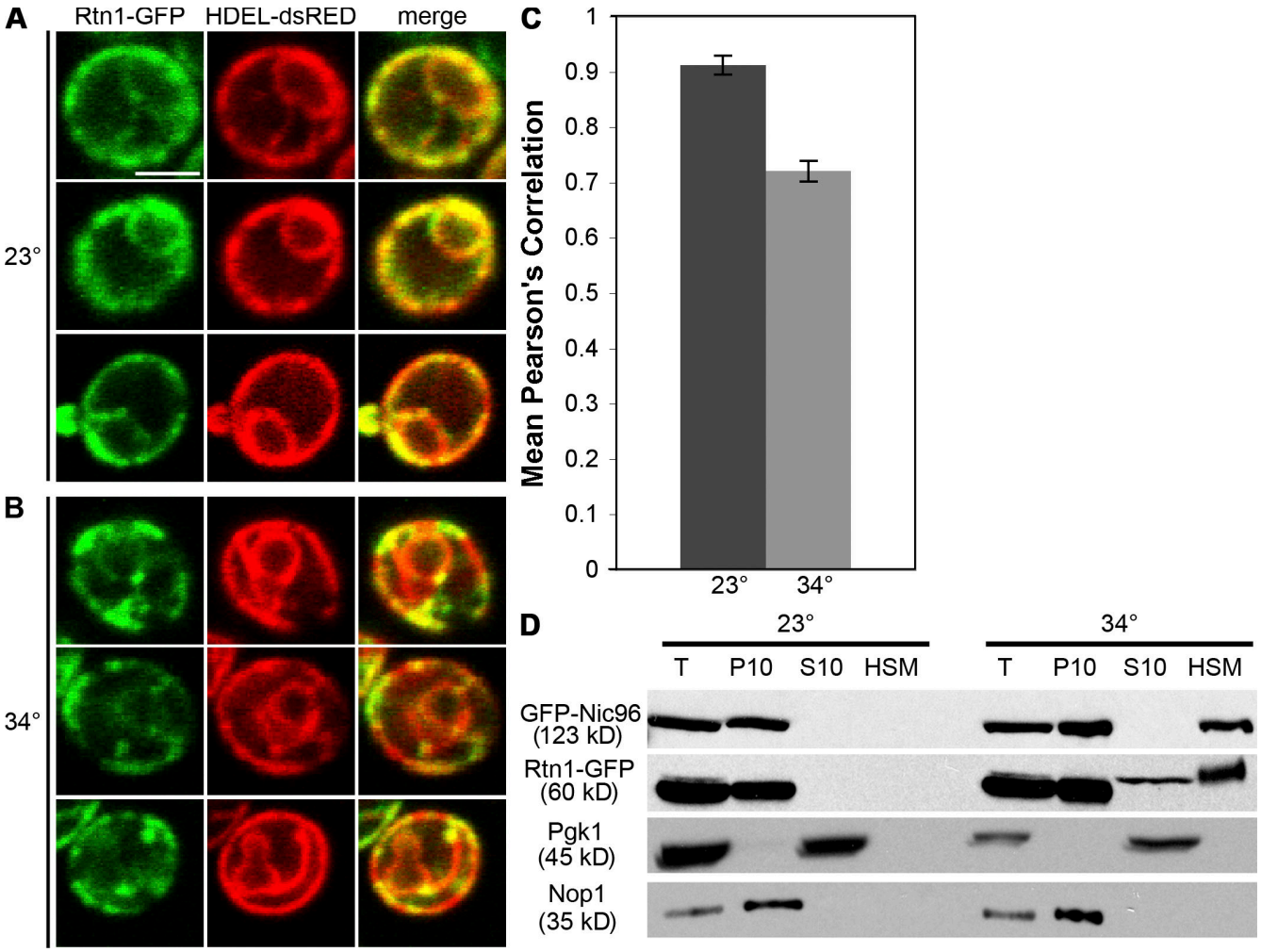

Figure 1. **Rtn1-GFP mislocalizes and is associated with an HSM fraction in the *prp20-G282S* assembly mutant.** (A and B) Rtn1-GFP and dsRed-HDEL localization in the *prp20-G282S* mutant background was visualized by direct laser-scanning confocal microscopy. The *prp20-G282S* mutant (SWY3747) was grown to early log phase (23°C; A) and shifted to 34°C for 5 h (B). Single-channel fluorescence is shown from three representative cells at each temperature, and merged images are shown (right). (C) Quantitative analysis of relative Rtn1-GFP and dsRed-HDEL distribution in *prp20-G282S* cells at 23 and 34°C. n = 12 cells for each respective Pearson's coefficient of correlation (+1.0 = complete coincidence; −1.0 = no coincidence). Error bars represent standard deviation. (D) Biochemical fractionation was performed with *rtn1-GFP GFP-nic96 prp20-G282S* cells (SWY3748) grown to early log phase (23°C) and shifted to 34°C for 5 h. After lysis, subcellular fractionation was performed by differential centrifugation. Cellular equivalent fractions of the total lysate (T), pellet (P; 10,000 *g*), and supernatant (S; 10,000 *g*) fractions and 10 times the cellular equivalent of the HSM fraction (135,000-*g* pellet from the supernatant fraction) were separated by SDS-PAGE, transferred to nitrocellulose, and analyzed by immunoblotting with an anti-GFP. Distributions of cytoplasmic Pgk1 and nucleolar Nop1 were analyzed as controls. Bar, 2.5 µm.

localization (Geng et al., 2005; De Craene et al., 2006; Voeltz et al., 2006). However, after temperature shifting to 34°C, the Rtn1-GFP signal was redistributed (Fig. 1 B). Rtn1-GFP was localized in cytoplasmic and perinuclear foci, and there were notable regions of dsRed-HDEL–labeled peripheral ER that lacked Rtn1-GFP. To quantify relative colocalization, the mean Pearson's coefficient of correlation was calculated (Fig. 1 C). At 23°C, the Rtn1-GFP colocalization with dsRed-HDEL scored a mean Pearson's coefficient of ∼0.91. At 34°C, the mean Pearson's coefficient of correlation dropped to ∼0.72. Thus, the degree of overlap between Rtn1-GFP and dsRed-HDEL was significantly less in the temperature-arrested *prp20-G282S* cells. At the nonpermissive growth temperature, Yop1-GFP also showed a similar redistribution in the *prp20-G282S* mutant from cortical ER at 23°C to cytoplasmic regions at 34°C (Fig. S1 A, available at http://www.jcb.org/cgi/content/full/jcb.200806174/DC1). However, not all ER proteins were perturbed, as Sec63-GFP was not altered in the arrested *prp20-G282S* cells (Fig. S1 B).

We previously found that GFP-Nic96, an essential Nup, is associated with 80–100-nm cytoplasmic vesicles in the *prp20-G282S* mutant (Ryan et al., 2003). Thus, we conducted biochemical subcellular fractionation experiments for Rtn1-GFP in the *prp20-G282S* mutant. Total cell lysates from a *prp20-G282S GFP-nic96 rtn1-GFP* strain were prepared and fractionated by differential velocity centrifugation. Immunoblotting for nucleolar Nop1 and cytoplasmic Pgk1 confirmed nuclear fractionation (Fig. 1 D). In lysates from cells grown at the permissive temperature, both Rtn1-GFP and GFP-Nic96 were associated exclusively with the low-speed (10,000 *g*) pellet containing nuclei and ER membranes. However, after the temperature shift to 34°C, a significant fraction of Rtn1-GFP was redistributed from the low-speed pellet into the supernatant.

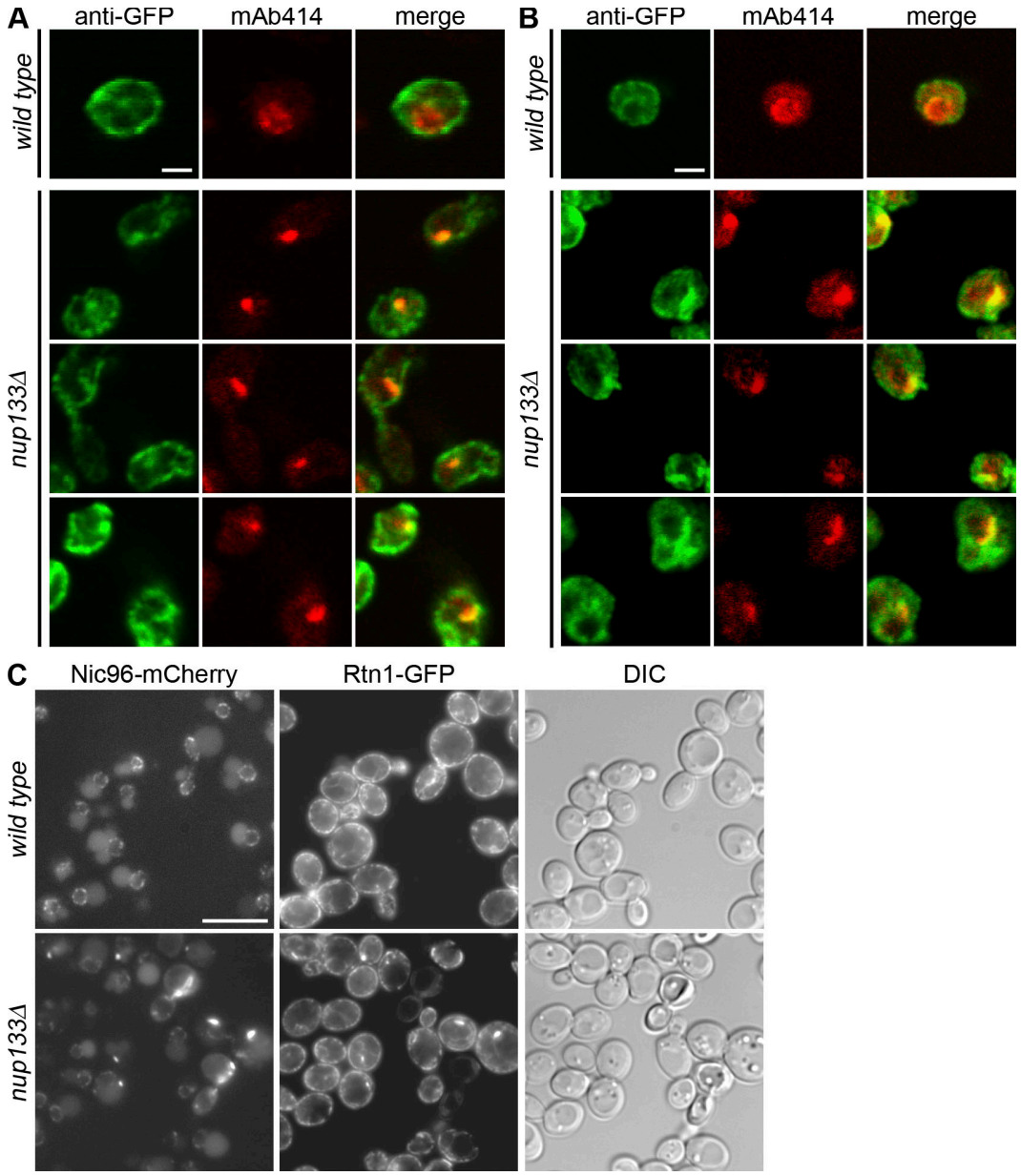

Figure 2. **Rtn1-GFP and Yop1-GFP are associated with NPC clusters in the *nup133Δ* mutant.** (A and B) Indirect immunofluorescence microscopy was conducted with parental *rtn1-GFP* cells (A, top), *nup133Δ rtn1-GFP* cells (SWY4007; A), parental *yop1-GFP* cells (B, top), or *nup133Δ yop1-GFP* cells (SWY4045; B) grown to early log phase at 23°C using rabbit anti-GFP and mouse anti–FG Nup mAb414 antibodies. Direct laser-scanning confocal microscopy was used with single-channel fluorescence for the GFP and mAb414 staining shown from three representative fields. Merged images are shown (right). (C) Live cell direct fluorescence microscopy was conducted with *rtn1-GFP nic96-mCherry* (SWY4125) and *rtn1-GFP nic96-mCherry nup133Δ* cells (SWY2117) grown to early log phase at 23°C. DIC, differential interference contrast. Bars: (A and B) 2.5 µm; (C) 10 µm.

Moreover, Rtn1-GFP and GFP-Nic96 were observed in a high-speed (135,000 *g*) membrane fraction. We concluded that blocking NPC assembly at the RanGTPase step perturbed Rtn1-GFP and Yop1-GFP localization.

Rtn1-GFP and Yop1-GFP localize to NPC clusters in a *nup133Δ* mutant

Recent studies of RTN and Yop1/DP1 localization in yeast and metazoan cells report enrichment in the cortical ER (Geng et al., 2005; De Craene et al., 2006; Voeltz et al., 2006; Shibata et al., 2008). One classical approach to define whether factors are physically associated with NPCs is to test for colocalization with NPC clusters in a *nup133Δ* mutant. Indirect immunofluorescence microscopy was performed on *nup133Δ rtn1-GFP* and *nup133Δ yop1-GFP* cells, and confocal microscopy revealed colocalization of a fraction of Rtn1-GFP with anti-FG (phenylalanine glycine repeat motif) Nups in large nuclear rim–associated clusters (Fig. 2 A). Similar colocalization in NPC clusters was observed for Yop1-GFP in *nup133Δ yop1-GFP* cells (Fig. 2 B). To confirm the Rtn1-NPC colocalization, we also analyzed live *nic96-mCherry rtn1-GFP nup133Δ* cells by direct fluorescence microscopy (Fig. 2 C). Foci of Rtn1-GFP were coincident with the Nic96-mCherry clusters. Of note, previous studies have shown that several other ER/NE-associated integral membrane

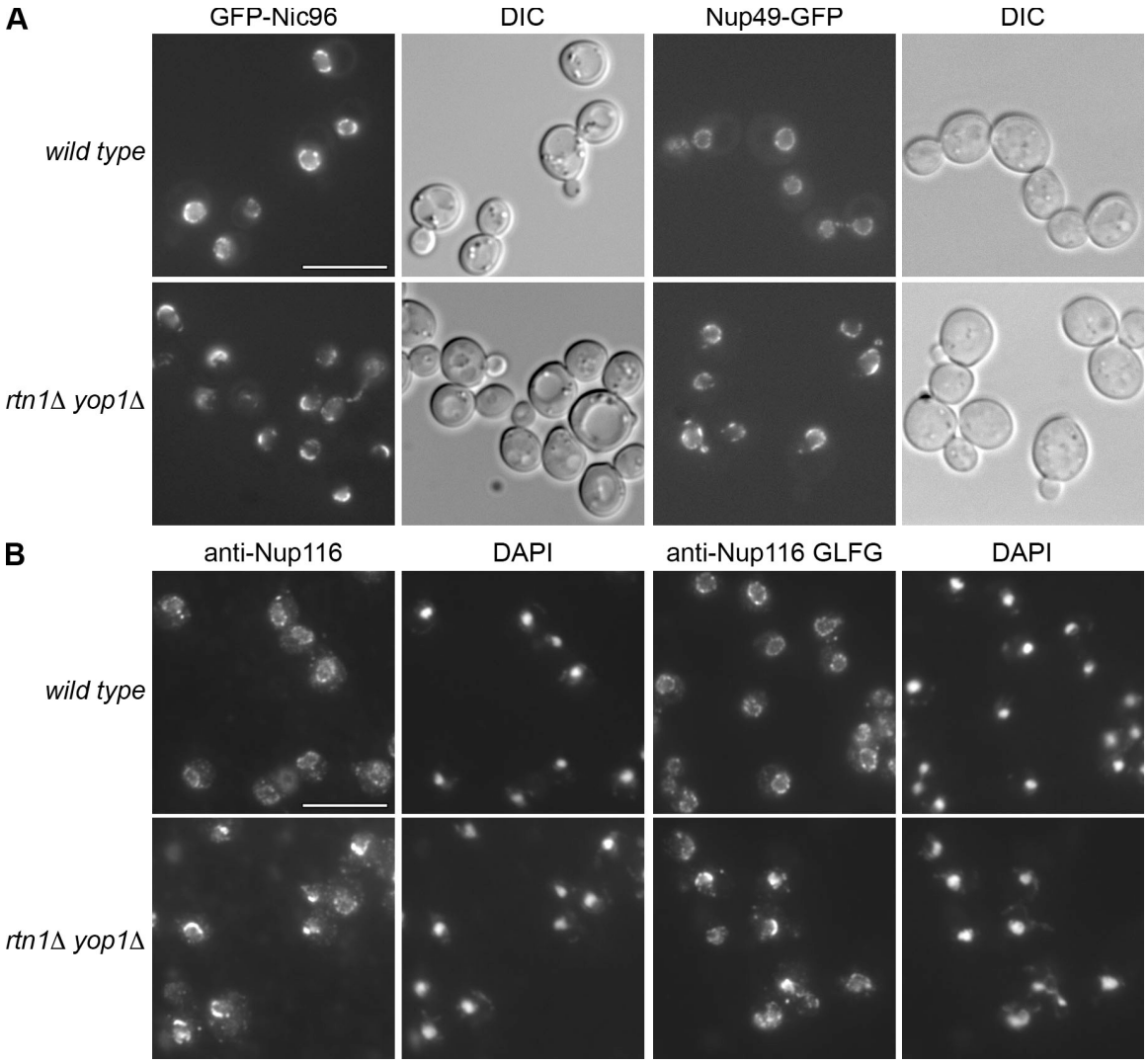

Figure 3. **Nups mislocalize in the *rtn1Δ yop1Δ* mutant.** (A) Parental cells (SWY1695 or SWY809) or *rtn1Δ yop1Δ* cells expressing either GFP-Nic96 or Nup49-GFP (SWY3931 or SWY3880) were grown to early log phase at 23°C and were visualized by direct fluorescence microscopy. (B) Parental cells (BY4742) or *rtn1Δ yop1Δ* cells (SWY3811) were grown to early log phase at 23°C and processed for indirect immunofluorescence microscopy with anti-Nup116C or anti–Nup116-GLFG antibodies. Nuclei were detected with the DNA dye DAPI. DIC, differential interference contrast. Bars, 10 μm.

proteins are not detected at NPC clusters (Siniossoglou et al., 1998; de Bruyn Kops and Guthrie, 2001; Baker et al., 2004; Scarcelli et al., 2007). Thus, these results provided evidence of a functional or physical link for Rtn1 and Yop1 with NPCs.

Rtn1 and Yop1 are required for normal Nup localization

To investigate whether Rtn1 and/or Yop1 is involved in NPC structure and function, we tested whether Rtn1 or Yop1 was required for proper Nup localization. *RTN1* and *YOP1* are not essential in *S. cerevisiae*, and neither is the closely related *RTN2* that is expressed at lower relative levels under normal growth conditions (Oertle et al., 2003). Others have reported *rtn1Δ* and *rtn1Δ yop1Δ* mutants with defects in peripheral ER morphology (De Craene et al., 2006; Voeltz et al., 2006). However, these studies did not examine NPC structure or localization. The *rtn1Δ*, the *yop1Δ*, and the *rtn1Δ yop1Δ* mutant strains were analyzed by direct fluorescence microscopy of chromosomally integrated *GFP-nic96* or *nup49-GFP*. In wild-type cells, the GFP-tagged Nups localized in a punctate pattern around the entire nuclear rim (Fig. 3 A). GFP-tagged Nup localization in individual *rtn1Δ* and *yop1Δ* mutants was not perturbed (unpublished data). However, a striking pattern of Nup mislocalization was observed in the *rtn1Δ yop1Δ* double mutant (Fig. 3 A). For both GFP-Nic96 and Nup49-GFP, the majority of the signal was concentrated in distinct nuclear rim foci.

We also performed indirect immunofluorescence for Nup116 and the FG Nup family. In wild-type cells, Nup116 and the FG Nups exhibit punctate staining around the entire nuclear rim (Fig. 3 B). However, in the *rtn1Δ yop1Δ* mutant cells, both anti-Nup116–specific and anti–GLFG (glycine leucine FG) Nup staining was concentrated in discrete foci at the nuclear rim. Similar results were obtained with the anti–FxFG Nup

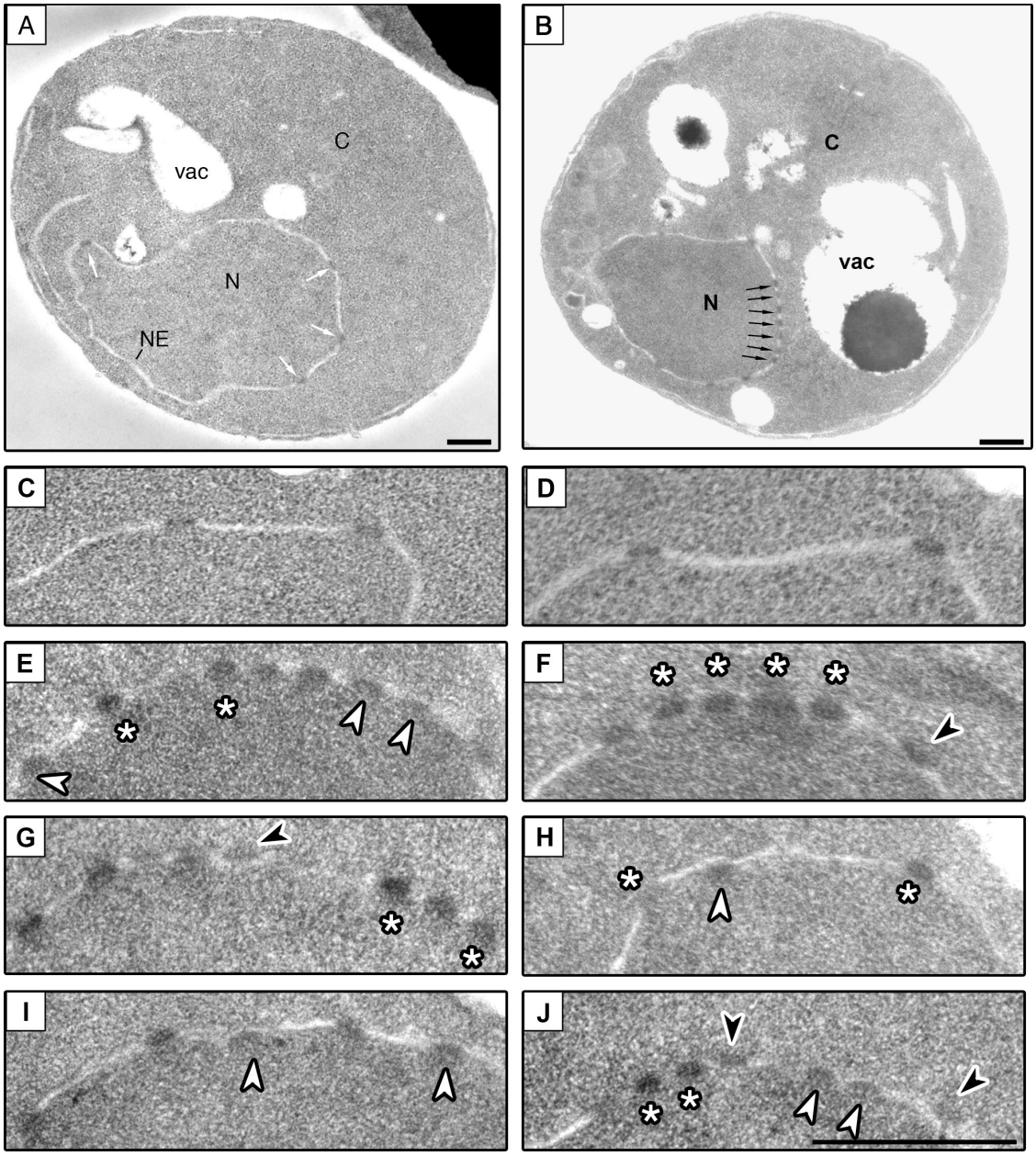

Figure 4. **NPCs are clustered and morphologically abnormal in *rtn1Δ yop1Δ* cells.** (A–J) Parental cells (BY4742; A, C, and D) or *rtn1Δ yop1Δ* cells (SWY3811; B and E–J) were grown to early log phase at 23°C and processed for thin-section EM. Black and white arrows point to the NPC, black arrowheads point to NPC-like structures at the ONM, white arrowheads point to NPC-like structures at the INM, and the asterisks denote other aberrant NPC-like structures at the NE. N, nucleus; C, cytoplasm; vac, vacuole. Bars, 0.5 µm.

mouse mAb414 (unpublished data). Overall, the mislocalization of both structural and peripheral Nups in the *rtn1Δ yop1Δ* mutant indicated potential perturbations in NE morphology, NPC distribution, NPC assembly, and/or structural stability.

NPC morphology and distribution are altered in the *rtn1Δ yop1Δ* mutant

The ultrastructure of an *rtn1Δ* mutant has no reported defects in NE morphology (De Craene et al., 2006). To evaluate *rtn1Δ yop1Δ* cells, we performed thin-section EM using methods to detect the electron densities representing NPCs. Wild-type NPCs in the parental strain appeared as electron-dense structures spanning the plane of the INM and ONM and were distributed evenly around the NE rim (Fig. 4, A [arrows], C, and D). In contrast, *rtn1Δ yop1Δ* mutant cells exhibited a range of striking defects in NPC structure and distribution (Fig. 4, B and E–J). Consistent with the concentrated Nup foci observed by fluorescence microscopy (Fig. 3), NPCs were clustered in a limited NE region (Fig. 4 B). Within these NPC clusters, some electron-dense structures similar to wild-type NPCs were found (~35% of the population). Interestingly, in *rtn1Δ yop1Δ* cells, there was a significant fraction of NE-associated electron-dense structures that did not fully span the INM/ONM plane. Approximately 30% of the electron-dense structures were associated with only one side of the NE, with 20% confined to the INM face (Fig. 4, E and H–J, white arrowheads), and 10% localized at the ONM face (Fig. 4, F, G, and J, black arrowheads).

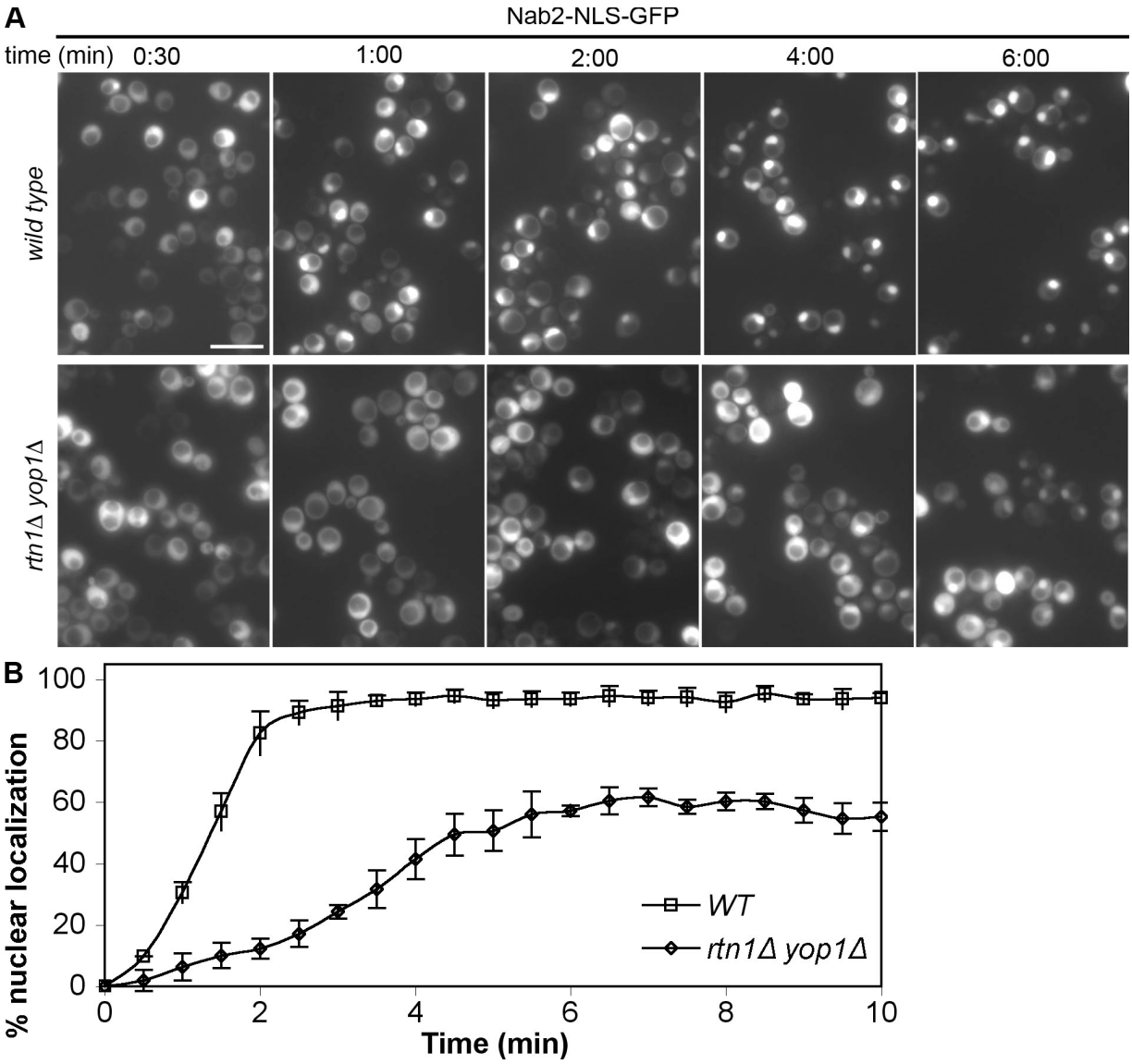

Figure 5. **The *rtn1Δ yop1Δ* mutant has Nab2NLS-GFP nuclear import defects.** Parental (BY4742) and *rtn1Δ yop1Δ* (SWY3811) cells with a plasmid expressing Nab2NLS-GFP (pNS167; Shulga et al., 2000) were grown to early log phase at 23°C. Import kinetics were determined after shifting energy-depleted cells with cytoplasmic Nab2NLS-GFP to glucose-containing media. (A) Localization of Nab2NLS-GFP by direct fluorescence microscopy at time points (minutes) after reinitiating import. (B) Kinetic data for three independent trials. Error bars represent standard deviation. Bar, 10 μm.

Overall, the NPC clusters in the *rtn1Δ yop1Δ* cells most closely resembled the NPC clusters reported in the *nup133/rat3-1* mutant (Li et al., 1995). The *rtn1Δ yop1Δ* NE/NPC structure was distinctly different from the herniated clustered NPCs in *apq12Δ*, *brr6-1*, and *nup116Δ* mutants (Wente and Blobel, 1993; de Bruyn Kops and Guthrie, 2001; Scarcelli et al., 2007), the grapelike NE-NPC clusters in *nup145*, *nup84*, and *nup85* mutants (for review see Doye and Hurt, 1997), and the extended ER/NE in *spo7Δ* and *nem1Δ* mutants (Siniossoglou et al., 1998). The morphological aberrancies in the *rtn1Δ yop1Δ* mutant cells confirmed defects in NPC distribution, assembly, and/or maintenance.

Nuclear import defects are detected in the *rtn1Δ yop1Δ* mutant

If NPC assembly and/or stability is perturbed in the *rtn1Δ yop1Δ* mutant, nuclear transport efficiency might also be inhibited. Nuclear import is mediated in a signal-dependent manner by the Kap transport receptor family (Terry et al., 2007), with effective import rates for different family members dependent on their cellular abundance (Timney et al., 2006). Using established transport assays (Strawn et al., 2004; Terry and Wente, 2007), we tested the Kap95, Kap104, and mRNA export pathways for defects in the *rtn1Δ yop1Δ* mutant cells. By in situ hybridization for poly(A)$^+$ RNA, nuclear accumulation was not observed, and mRNA export was not significantly inhibited (unpublished data). For the Kap import pathways, respective plasmids expressing GFP fusions to either the lysine-rich classical NLS from SV40 large T antigen or the Nab2NLS were transformed into the yeast strains. For the most abundant Kap, Kap95 (Timney et al., 2006), no steady-state import defects were observed with the classical NLS-GFP reporter (unpublished data). However, for Kap104, which has

an almost 10-fold lower abundance and a lower wild-type import rate efficiency (Timney et al., 2006), import of its model cargo Nab2NLS-GFP was inhibited (Fig. 5). Because cytoplasmic levels of Nab2NLS-GFP were elevated in the *rtn1Δ yop1Δ* mutant cells at steady state (unpublished data), we directly measured apparent import rates using an established assay for monitoring Nab2NLS-GFP import in live cells (Shulga et al., 1996). Cells were incubated in glucose-free media containing 10 mM 2-deoxy-D-glucose and 10 mM sodium azide, inhibiting active nuclear import and resulting in cytoplasmic redistribution of Nab2NLS-GFP. At time 0, cells were washed into glucose-containing media. At respective time points, nuclear versus cytoplasmic localization was scored by direct fluorescence microscopy (Fig. 5 A). In wild-type cells, Nab2NLS-GFP was rapidly reimported. In contrast, the *rtn1Δ yop1Δ* mutant cells had an approximately fourfold reduction in the relative import rate (Fig. 5 B). Thus, NE transport capacity in the *rtn1Δ yop1Δ* mutant cells was perturbed, which is consistent with the reduced number of apparently properly inserted NPCs (~35% of total; as discussed in the previous section and shown in Fig. 4).

The *rtn1Δ yop1Δ* mutant genetically interacts with mutants in genes encoding Poms and a subset of Nups

To further test for functional connections between NPCs and Rtn1 and/or Yop1, we systematically combined the *rtn1Δ* and *yop1Δ* mutants with a panel of viable *nup* mutants, *pom* mutants, and mutants for genes encoding ER/NE proteins with published perturbations of NE/NPC structure. Double, triple, and quadruple mutants were constructed bearing *URA3/CEN* plasmids with a wild-type allele for the respective *NUP*, *POM*, or *RTN1*. These strains were assayed for growth defects and synthetic lethality on rich media and 5-fluoroorotic acid (5-FOA) media at temperatures from 16 to 37°C.

Based on studies demonstrating a requirement for the vNup107–160 subcomplex in de novo NPC formation (D'Angelo et al., 2006) and suggesting that the conserved heptameric yNup84 subcomplex is involved in NPC assembly (Siniossoglou et al., 1996), we generated *rtn1Δ yop1Δ* mutant combinations with yNup84 subcomplex *nup* mutants. Triple mutant *rtn1Δ yop1Δ nup85Δ* cells were not viable without the *NUP85/URA3/CEN* plasmid (Table I, Fig. 6 A, and Fig. S2 A, available at http://www.jcb.org/cgi/content/full/jcb.200806174/DC1). Likewise, the *rtn1Δ yop1Δ nup120Δ* mutant and the *rtn1Δ yop1Δ nup145-R4^{ts}* mutant showed enhanced lethality and were severely compromised for growth. The *nup145-33* mutant expressing only the essential region of Nup145 (Emtage et al., 1997) was also not sufficient to support viability of the *rtn1Δ yop1Δ* mutant. Interestingly, yNup85, yNup120, and yNup145C are each required for assembly of the yNup84 subcomplex (Siniossoglou et al., 2000) and interact to form the heterotrimeric Y-shaped core of the yNup84 subcomplex structure (Lutzmann et al., 2002). In contrast, yNup84 and yNup133 form the stalk on the Y-shaped yNup84 subcomplex, and the *rtn1Δ yop1Δ nup133Δ* and *rtn1Δ yop1Δ nup84Δ* triple mutants were viable. No synthetic fitness defects were observed by combining the *rtn1Δ yop1Δ* mutant and *nup* mutants for peripheral FG Nups (*nup57^{ts}*, *nup100Δ*, *nup42Δ*, *nup60Δ*, *nup1Δ*, and *nup2Δ*; Table I). These data were consistent with the hypothesis that Rtn1 and/or Yop1 plays coordinated roles with specific yNup84 subcomplex functions.

Roles for the Poms in pore formation and stabilization have been proposed (for review see Antonin et al., 2008); however, degrees of functional redundancy exist among the yeast Poms (Madrid et al., 2006; Miao et al., 2006). Neither the *pom34Δ* nor the *pom152Δ* mutant alone exhibited synthetic lethality in combination with the *rtn1Δ yop1Δ* mutant (Table I, Fig. S2 B). Strikingly, a quadruple *rtn1Δ yop1Δ pom34Δ pom152Δ* mutant strain was inviable (Table I, Fig. 6 A, and Fig. S2 B). This revealed a functional linkage between Rtn1-Yop1 and the Poms and further indicated that yNdc1 alone was not sufficient to support NPC structure and assembly and cell viability.

The Poms have been functionally linked to two other sets of Nups (Aitchison et al., 1995; Nehrbass et al., 1996; Marelli et al., 1998; Mansfeld et al., 2006; Miao et al., 2006; Alber et al., 2007b): one set referred to as linker Nups (Nup82 and Nic96 with links to Nup116 and Gle2) and another set of inner ring Nups (Nup170, Nup157, Nup188, and Nup192 with links to Nup53 and Nup59). We found synthetic or enhanced lethality for *nup82^{ts}*, *nup116Δ*, or *gle2Δ* mutants combined with the double *rtn1Δ yop1Δ* deletions and for *nup188Δ*; however, the *rtn1Δ yop1Δ nup* triple mutants with *nup170Δ*, *nup53Δ*, or *nup59Δ* were viable (Table I). Triple mutants with *nic96-1* and *nup159-1/rat7-1* temperature-sensitive alleles also showed no enhanced lethality. Overall, there were discrete *rtn1Δ yop1Δ* genetic interactions with mutants for defects in specific Nup subcomplexes.

Finally, we tested the effects of combining the *rtn1Δ yop1Δ* alleles with mutants in genes for non-NPC ER/NE proteins. Of note, triple mutants from the *rtn1Δ yop1Δ* combination with an *apq12Δ*, a *brr6-1*, or an *snl1Δ* allele were viable at all temperatures tested. In contrast, triple *rtn1Δ yop1Δ spo7Δ* and *rtn1Δ yop1Δ nem1Δ* mutants were severely compromised for growth on 5-FOA (Table I). Spo7 and Nem1 comprise an ER/NE-localized phosphatase complex that negatively regulates phospholipid biosynthesis (Siniossoglou et al., 1998; Santos-Rosa et al., 2005). Increased phospholipid biosynthesis in *spo7Δ* or *nem1Δ* cells perturbs the ER and NE, although NPC function is apparently intact (Siniossoglou et al., 1998; Campbell et al., 2006). Combining the *nup84Δ* mutant with an *spo7Δ* or an *nem1Δ* allele results in lethality; however, the *spo7Δ* and *nem1Δ* mutants are not genetically linked to *nup85Δ* or *pom152Δ* (Siniossoglou et al., 1998). This contrasted with our results showing no effect of the *rtn1Δ yop1Δ* combination with the *nup84Δ* allele but specific lethality with the *nup85Δ* and the *pom152Δ pom34Δ* mutants. Collectively, this suggested potential distinct roles for Rtn1-Yop1 and Spo7-Nem1 at the ER and NE/NPC.

Genetic suppression links between Rtn1 function and the Poms

Rtn1 and Yop1 are enriched in the tubular ER; however, a recent study reported the isolation of an *rtn1-K48I* mutant with predominant NE localization, defects in oligomerization, and increased membrane mobility (Shibata et al., 2008). Rtn1 oligomerization is thought to be required for ER tubule formation

Table I. **Genetic interactions with *rtn1Δ yop1Δ***

Genotype	Genetic interaction	Growth on 5-FOA	Growth on YPD				
			16°C	23°C	30°C	34°C	37°C
rtn1Δ yop1Δ	NA		+	+	+	+	+
Nup84 subcomplex							
nup85Δ	NA	+	+	+	+	−	−
nup85Δ rtn1Δ yop1Δ	synthetic lethal	−	−	−	−	−	−
nup120Δ	NA	+	+	+	+	+	−
nup120Δ rtn1Δ yop1Δ	synthetic sick	−+	−+	−+	−+	−+	−
nup145Δ + pNUP145-R4Δ1-1090	NA	+	+	+	+	+	−
nup145Δ rtn1Δ yop1Δ + pNUP145-R4	enhanced lethality	+	+	+	−+	−−+	−
nup145Δ + pNUP145-33	NA	+	+	+	+	+	−
nup145Δ rtn1Δ yop1Δ + pNUP145-33	synthetic lethal	−	−	−	−	−	−
Poms							
pom34Δ rtn1Δ yop1Δ	none	+	+	+	+	+	+
pom152Δ rtn1Δ yop1Δ	enhanced lethality	+	−+	+	+	+	−+
pom34Δ pom152Δ rtn1Δ yop1Δ	synthetic lethal	−	−	−	−	−	−
Linker Nups							
nup82-3	NA	+	+	+	+	+	−
nup82-3 rtn1Δ yop1Δ	synthetic lethal	−	−	−	−	−	−
nup116Δ	NA	+	+	+	+	+	−
nup116Δ rtn1Δ yop1Δ	synthetic sick	−−+	−−+	−−+	−−+	−−+	−
gle2Δ	NA	+	+	+	+	+	−
gle2Δ rtn1Δ yop1Δ	synthetic lethal	−	−	−	−	−	−
Core Nups							
nup188Δ	NA	+	+	+	+	+	+
nup188Δ rtn1Δ yop1Δ	synthetic lethal	−	−	−	−	−	−
INM proteins							
spo7Δ	NA	+	+	+	+	+	−+
spo7Δ rtn1Δ yop1Δ	synthetic sick	−−+	−+	−+	−+	−+	−−+
nem1Δ	NA	+	+	+	+	+	−+
nem1Δ rtn1Δ yop1Δ	synthetic sick	−−+	−−+	−−+	−−+	−−+	−−+

rtn1Δ yop1Δ triple mutants showing no enhanced growth defects included *nup84Δ*, *nup133Δ*, *nup145ΔN*, *snl1Δ*, *nup53Δ*, *nup170Δ*, *nup59Δ*, *brr6Δ/brr6-1*, *apq12Δ*, *nup57-E17*, *nup159-1/rat7-1*, *nic96-1*, *nup1Δ*, *nup2Δ*, *nup60Δ*, *nup42Δ*, and *nup100Δ*. Synthetic lethal and synthetic sick strains were maintained with a URA3/CEN plasmid carrying wild-type copies of *NUP85*, *NUP120*, *NUP145*, *POM34*, *NUP116*, *GLE2*, or *NUP188* or a wild-type copy of RTN1 for *spo7Δ*, *nem1Δ*, and *nup82-3* triple mutants. Synthetic lethality indicates failure to grow on 5-FOA; synthetic sickness indicates moderate to severe growth inhibition on 5-FOA. Enhanced lethality indicates increased temperature sensitivity of 5-FOA–resistant *ura*$^-$ isolates grown on YPD (1% yeast extract, 2% peptone, and 2% dextrose) at the given temperatures. +, growth; −+, moderate growth inhibition; −−+, severe growth inhibition; −, no growth at the indicated temperature.

(Hu et al., 2008; Shibata et al., 2008). We used this *rtn1-K48I* mutant to test whether the Rtn1 connection to NPCs was via an ER tubule or an NE role. Expression of *rtn1-K48I* fully rescued the clustering of NPCs in the *rtn1Δ yop1Δ* mutant cells (Fig. S3, available at http://www.jcb.org/cgi/content/full/jcb.200806174/DC1) and the *rtn1Δ yop1Δ pom34Δ pom152Δ* mutant lethality (not depicted). Furthermore, in testing a panel of previously generated *pom34Δ nupΔ* and *pom152Δ nupΔ* synthetic lethal mutants (Miao et al., 2006), we found that a *pom34Δ nup59Δ* lethal double mutant was partially rescued for growth by the presence of *RTN1/LEU2* or *rtn1-K48I/LEU2* plasmids (Fig. 6, B and C), with reproducibly more robust rescue by the *rtn1-K48I* expression. We concluded that predominant peripheral ER localization is not required for the Rtn1 role at the NE.

We also investigated whether overproducing the Poms would rescue the NPC clustering defect in *rtn1Δ yop1Δ* cells. Plasmids expressing *NDC1*, *POM152*, *POM34*, or *SNL1* were transformed into the *rtn1Δ yop1Δ* strain and the *rtn1Δ yop1Δ GFP-nic96* strain. NPC clustering was assessed in each of the transformed strains by direct fluorescence microscopy for GFP-Nic96 (Fig. 7 A) or by indirect immunofluorescence microscopy with anti–Nup116-GLFG antibodies (Fig. 7 B). Exogenous expression of *NDC1* clearly decreased the appearance of NPC clusters, with *POM152* also rescuing but to a lesser extent (Fig. 7). In contrast, the clustering phenotype was not efficiently rescued by exogenous plasmid expression of *POM34* or *SNL1*, an ER membrane protein genetically linked to *NUP*s (Ho et al., 1998; Sondermann et al., 2002).

Rtn4a is required for de novo pore formation in vitro

Our results in the *S. cerevisiae* model suggested that Rtn1 and Yop1 are required for proper NPC distribution, structural stability, and/or biogenesis. To directly test for a role in NPC assembly, we turned to our recently established cell-free NPC insertion assay using *Xenopus* egg extracts (D'Angelo et al., 2006). Preassembled nuclei were formed by incubating sperm chromatin, cytosol, and isolated membranes for 60 min. To monitor de novo NPC biogenesis, preassembled nuclei were then incubated with fresh cytosol for an additional 30-min period, during which the NE expands and NPC insertion occurs at a rate of ∼150 NPCs/min (D'Angelo et al., 2006). A previously

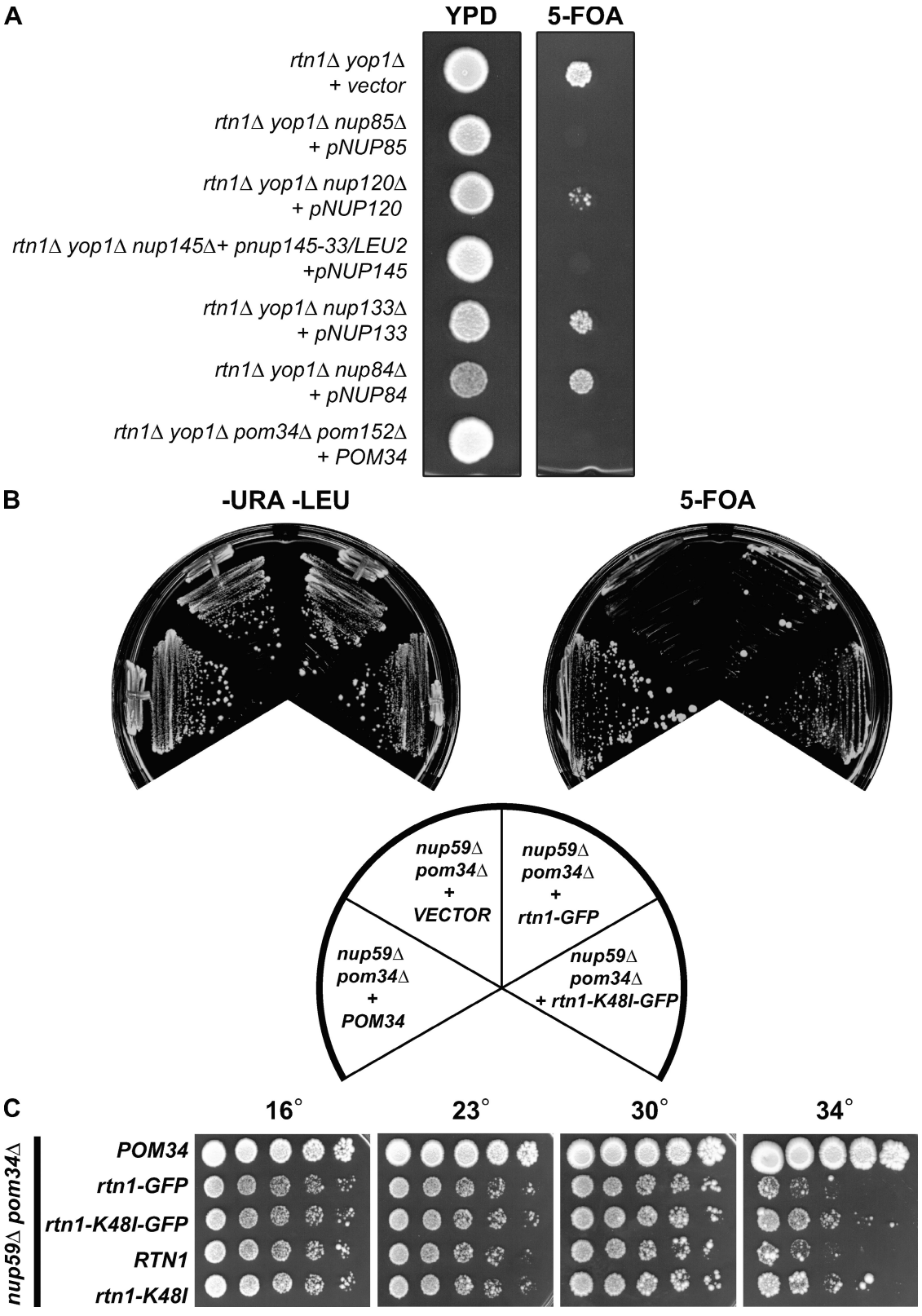

Figure 6. **Genetic interactions for the *rtn1Δ yop1Δ* mutant with mutants in genes encoding Nups, Poms, and ER/NE proteins.** (A) Analysis of *rtn1Δ yop1Δ nup/pom* mutants. Haploid strains with the designated chromosomal deletions and wild-type *RTN1*, *POM*, or *NUP URA3/CEN* plasmid were tested for growth on 5-FOA media (SWY3811 + pRS316, SWY3876 + pSW3354, SWY3877 + pSW1079, SWY3878 + pSW1516, SWY4050 + pSW351, SWY4099 + pSW610, and SWY4106 + pSW3459). (B) Rescue of *pom34Δ nup59Δ* cells (SWY3139) by exogenous expression of *RTN1-GFP* or *rtn1-K48I–GFP*. The *pom34Δ nup59Δ* parental strain harboring a *POM34/URA3* plasmid and *LEU2* plasmids for *POM34*, *RTN1-GFP*, or *rtn1-K48I–GFP* were assayed for growth on 5-FOA media (23°C for 6 d). (C) Growth of 5-FOA–resistant *pom34Δ nup59Δ* isolates expressing *POM34*, *rtn1-GFP*, *rtn1-K48I–GFP*, *RTN1*, or *rtn1-K48I* was assessed after serial dilution on YPD.

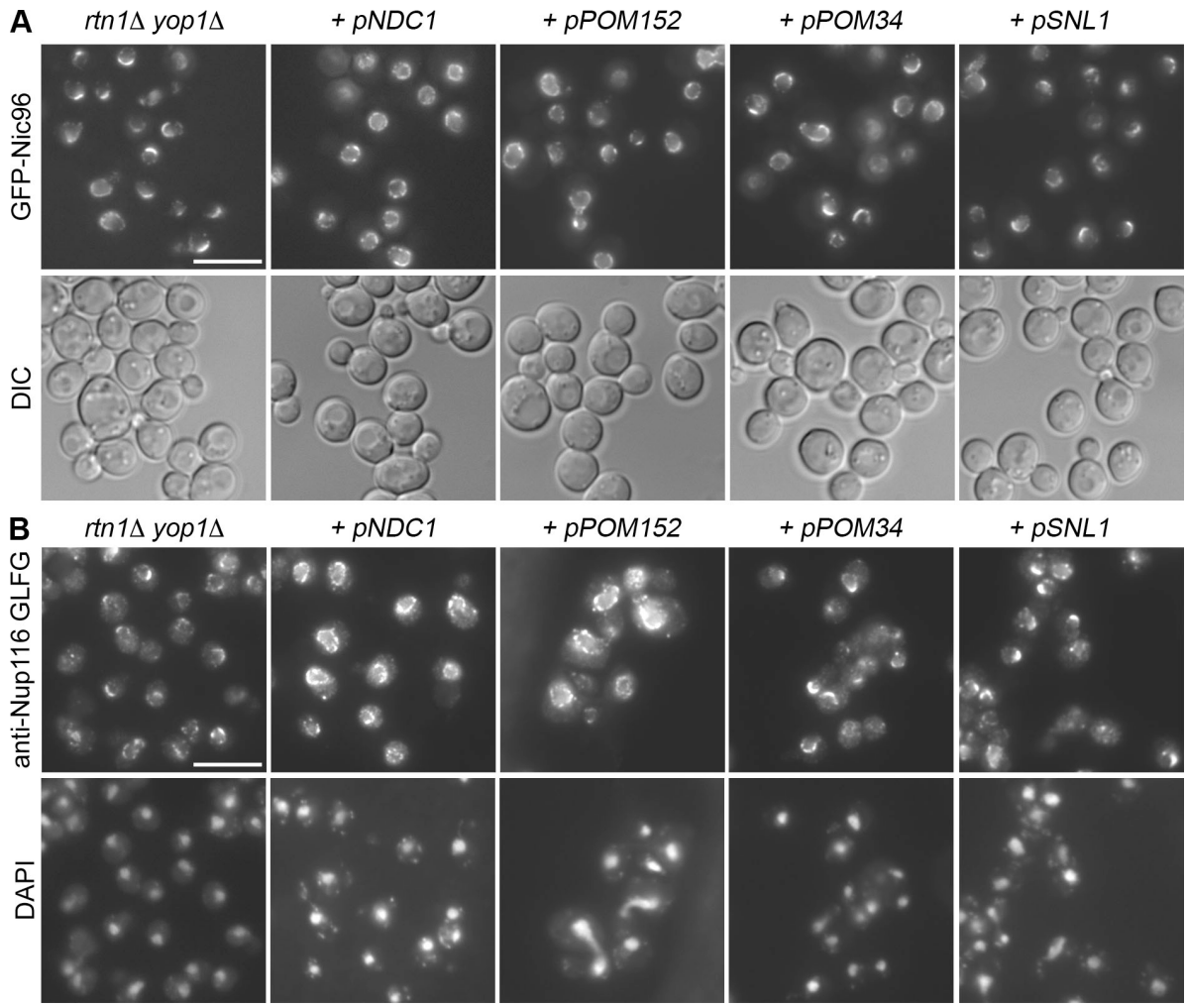

Figure 7. **Exogenous expression of Ndc1 and Pom152 rescues the *rtn1Δ yop1Δ* Nup mislocalization phenotype.** (A and B) The *rtn1Δ yop1Δ GFP-nic96* (SWY3931; A) and the *rtn1Δ yop1Δ* (SWY3811; B) strains were transformed with plasmids expressing *NDC1* (pRS315.NDC1; Chial et al., 1998), *POM152* (pSW229), *POM34* (pSW1517; Miao et al., 2006), or *SNL1* (pSW575; Ho et al., 1998). Direct fluorescence microscopy (A) or indirect immunofluorescence microscopy with anti–Nup116-GLFG antibodies (B) was conducted to evaluate NPC clusters. DIC, differential interference contrast. Bars, 10 μm.

characterized specific inhibitory antibody against the cytosolic N-terminal domain of Rtn4a (Voeltz et al., 2006) was added, and we observed a strong block in the assembly of new pores (Fig. 8 A). No effect was observed with the addition of control or anti-Rtn2 antibodies (previously shown to be noninhibitory; Fig. 8 A; Anderson and Hetzer, 2007). Importantly, NE expansion was not significantly affected by the anti-Rtn4a antibody (Fig. S4 C, available at http://www.jcb.org/cgi/content/full/jcb.200806174/DC1). This indicated that tubular connections between the NE and the ER, which are required for NE growth (Anderson and Hetzer, 2007), were not disrupted. However, at later time points during the course of the experiment, the ER network slowly disintegrated into vesicles in the presence of the Rtn4a antibody (unpublished data), and the NE was inhibited, which is consistent with the previously published requirement of ER network for nuclear growth (Anderson and Hetzer, 2007; Kiseleva et al., 2007).

To further investigate whether the inhibition of NPC assembly is a consequence of RTN function in nuclear pore formation, we developed a sensitive method to functionally monitor the early steps of pore formation, i.e., INM/ONM fusion, as opposed to the appearance of fully assembled NPCs. This was based on a fluorescence microscopy assay in which the formation of new pores (i.e., holes in the NE) is detected by the influx of a fluorescently labeled 70-kD dextran. Under standard experimental conditions, intact NPCs are inserted into the NE pores of assembled nuclei, and a permeability barrier is coincidentally established that excludes molecules >60 kD (Fig. 8 B). However, when glycosylated Nups are depleted from the extracts using WGA, NPC assembly still occurs, but the pores exhibit a defective permeability barrier (Finlay and Forbes, 1990; Miller and Hanover, 1994). Thus, we depleted glycosylated Nups from the fresh cytosol before adding to preassembled nuclei (Fig. S4, A and B) and found that the fluorescent 70-kD dextran was present in the nucleus (Fig. 8, B and C). This was consistent with previous findings (Finlay and Forbes, 1990) and indicated that new pores formed, but they were defective in the permeability barrier function. To test whether the influx of 70-kD dextran was dependent on new

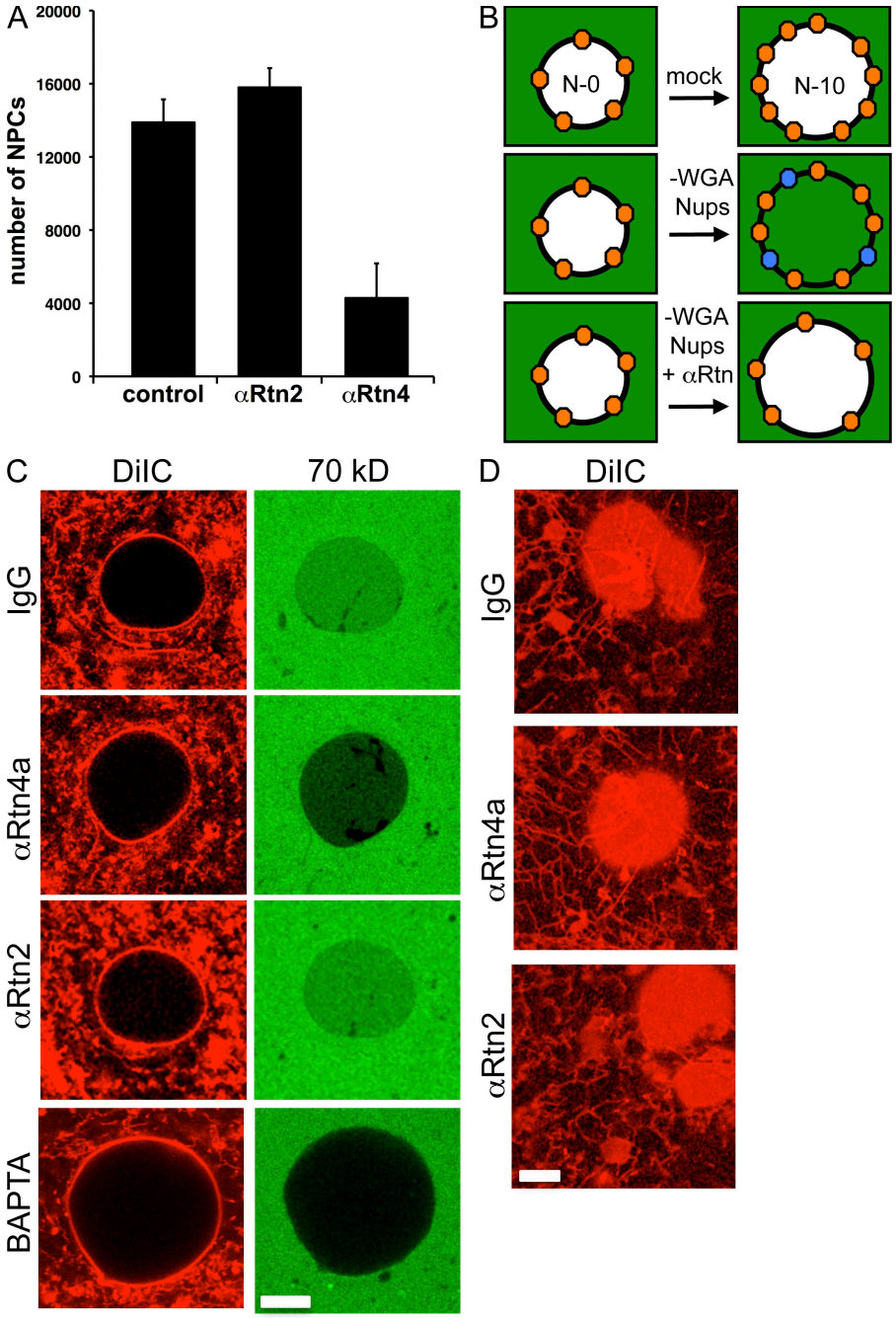

Figure 8. ***Xenopus* Rtn4a is required for de novo NPC formation in vitro.** (A) Inhibition of NPC insertion by anti–(α)-Rtn4a but not anti–(α)-Rtn2 antibodies. Preassembled nuclei were incubated with fresh cytosol in the presence of 10 µM of antibodies for 30 min, and pores were visualized by fluorescently labeled WGA. The NPC number of 50 nuclei is plotted. Error bars represent standard deviation. (B) Schematic illustration of dextran influx assay. When preassembled nuclei (N-0) are incubated with mock-depleted cytosol, intact new pores are inserted (orange circles). In contrast, when N-0 nuclei are incubated with WGA-depleted cytosol, new pores form that cannot exclude dextran (blue circles). If RTNs are required for an early step of NPC assembly, pore/hole formation should be blocked and 70-kD dextran should be excluded. (C) Nuclei were assembled with $DiIC_{16}(3)$-labeled membranes (red) and incubated with WGA-depleted cytosol in the absence (IgG and α-Rtn2) or presence of inhibitory antibodies (α-Rtn4a) or the calcium chelator BAPTA. After a 10-min incubation, fluorescently labeled 70-kD dextran was added (green), and nuclei were immediately imaged using confocal microscopy ($n \geq 20$). (D) In the same reactions as C, surface images were taken from unfixed nuclei that did not exclude (IgG and α-Rtn2) or did exclude (α-Rtn4a) 70-kD dextran. Under all conditions, the NEs were visible as flat membrane patches connected to intact ER tubules. Bars, 10 µm.

pore formation, we preassembled nuclei for 60 min and added WGA-depleted cytosol in the presence of BAPTA, a known inhibitor of NPC assembly (Macaulay and Forbes, 1996). Strikingly, under these conditions, the influx of 70-kD dextran was strongly inhibited (Fig. 8 C). Next, we analyzed whether RTNs were required for early steps of NPC assembly. We assembled nuclei for 60 min and added WGA-depleted cytosol in the absence or presence of inhibitory anti-Rtn4a antibody. In reactions with control antibodies, influx of 70-kD dextran was detected 5 min after the addition of WGA-depleted cytosol. In contrast, no influx was observed in the presence of anti-Rtn4a antibody (Fig. 8 C). Importantly, the tubular ER network remained intact during this same period of time (Fig. 8 D), suggesting that Rtn4a is required for the de novo assembly of new pores into the NE.

Discussion

In this study, we describe a novel connection for the ER proteins Rtn1 and Yop1 with nuclear pore and NPC biogenesis. Previous studies have restricted Rtn1 and Yop1 function to the tubular ER with no known roles at the NPC reported (Geng et al., 2005; De Craene et al., 2006; Voeltz et al., 2006; Shibata et al., 2008). Several lines of evidence support our conclusions. First, we observe perturbations in Rtn1-GFP localization in the NPC assembly mutant *prp20-G282S*. Second, Rtn1-GFP appears to concentrate at NPC clusters in a *nup133Δ* mutant. Third, the lack of Rtn1 and Yop1 results in clusters of NPC-like structures in localized regions of the NE. Fourth, our genetic results reveal a tight link between Rtn1/Yop1 function at the NE with the Poms, the linker

Nups, and the yNup84 subcomplex. Finally, using *Xenopus* in vitro assays for de novo NPC assembly, we find that anti-Rtn4a antibodies specifically inhibit pore biogenesis. We conclude that a combination of RTN, Yop1/DP1, and Poms is required for the formation of nuclear pores and/or the insertion of NPCs into the pore. We predict that these membrane-bending proteins influence the stability of the pore membrane during NPC biogenesis. These results directly impact current models for de novo pore formation and ER/NE membrane dynamics.

Our yeast genetic experiments uncover separable roles for different membrane proteins at the NE/NPC. Strikingly, Ndc1 is not sufficient for growth or, presumably, NPC assembly. This is based on the lethality of the *rtn1Δ yop1Δ pom34Δ pom152Δ* mutant. Furthermore, we find that the *rtn1Δ yop1Δ* double mutant has specific genetic interactions with genes encoding Nups in the yNup84 subcomplex and in the linker Nup subcomplex. In contrast, strong connections to the inner ring Nups are not detected. In regard to ER/NE proteins, a specialized NE and/or nuclear pore lipid composition and membrane fluidity might also be required (Schneiter et al., 1996; Scarcelli et al., 2007). However, the reported abnormalities in NE/NPC morphology for mutants in genes encoding other NE-associated integral membrane proteins, including Acc1, Apq12, Brr6, Spo7, and Nem1 (Schneiter et al., 1996; Siniossoglou et al., 1998; de Bruyn Kops and Guthrie, 2001; Scarcelli et al., 2007), are structurally distinct from those in the *rtn1Δ yop1Δ* mutant. Overall, our genetic results indicate that the Rtn1 and Yop1 role in nuclear pore biogenesis is separate from that for Apq12 and Brr6. Moreover, based on the genetic interactions with the *spo7Δ* and *nem1Δ* mutants, we speculate that Rtn1 and Yop1 have separable functional roles in tubular ER maintenance and in NE pore formation.

The RTNs and Yop1/DP1 exert their effects on tubular ER morphology through influencing membrane curvature and fusion events (De Craene et al., 2006; Voeltz et al., 2006; Hu et al., 2008; Shibata et al., 2008). Yeast (y)Rtn1 (or vRtn4a) interacts with yYop1 (vDP1), and both are membrane proteins with a similar predicted hairpin topology (Voeltz et al., 2006). It is proposed that their respective extended hydrophobic domains insert only into the outer ER membrane leaflet as oligomers. Their unusual wedge-shaped membrane spans presumably displace lipid head groups to induce and stabilize a highly curved membrane structure in a manner proposed by the classical bilayer couple hypothesis (Sheetz et al., 1976; Voeltz et al., 2006).

There are several models for how these membrane proteins mediate nuclear pore formation. A role strictly involving ER tubules formed by Rtn1 and Yop1 could underlie the NPC connections. Recent reports link the functions of metazoan RTNs in tubular ER maintenance to both premitotic NE disassembly and NE postmitotic reassembly (Anderson and Hetzer, 2007; Audhya et al., 2007). In addition, vRtn4a is localized to highly curved membrane junctions between cytoplasmic membranes and the ONM (Kiseleva et al., 2007). The Rtn1/Yop1 ER tubules might connect to the NE and trigger transient ONM curvature. The tubular ER might also be required for localized delivery of NPC precursors such as POMs to the NE. However, strikingly, the *Xenopus* in vitro assays (Fig. 8) demonstrate that new NPC and pore biogenesis is inhibited by anti-Rtn4a antibodies at times when tubular ER connections to the NE are intact. This further supports our conclusion that RTNs play roles in NPC formation that are distinct from their function in maintaining tubular ER.

We propose that the RTNs and/or Yop1/DP1 functions directly at the NE to facilitate NPC biogenesis. A fraction of yeast Rtn1 has been observed at the NE by both yRtn1-GFP imaging (Fig. 1; Geng et al., 2005) and vRtn4a immuno-EM (Kiseleva et al., 2007). Our genetic interaction results indicate that Rtn1 and Yop1 are specifically linked to discrete Nup and Pom subcomplexes and to only a subset of specific ER/NE proteins (Fig. 6). Thus, there is no pleiotropic defect in the delivery of integral membrane proteins to the NE/NPC in *rtn1Δ yop1Δ* mutants. Furthermore, we find that the lethal *pom34Δ nup59Δ* mutant is more efficiently rescued by the NE-enriched *rtn1-K48I* mutant, which also has decreased oligomerization and greater membrane mobility (Shibata et al., 2008). Collectively, with the *Xenopus* in vitro assembly data, we propose that yeast Rtn1 (vRtn4a) and Yop1 function in the NE to stabilize the highly curved nuclear pore membranes.

Fusion of the INM and ONM is thought to be facilitated largely by the Poms; however, RTNs and/or Yop1/DP1 might independently be involved in localized bending of the ONM or INM to assist fusion. Alternatively, RTNs and/or Yop1/DP1 might be recruited after fusion to the nascent highly curved membrane, with their topological insertion into only the outer leaflet of the pore membrane, resulting in a stabilized nascent pore. In either of these scenarios, a physical interaction between the RTNs and/or Yop1/DP1 with NPC components is not necessarily required. Of note, a genome-wide split ubiquitin two-hybrid screen has reported an uncharacterized Yop1–Pom34 interaction (Miller et al., 2005). The colocalization of yeast Rtn1 and Yop1 with NPC clusters in *nup133Δ* cells could reflect a physical Pom–Nup interaction and a role at preexisting NPCs. However, proteomic studies have not reported the coisolation of Rtn1 or Yop1 with wild-type detergent-solubilized yeast NPC or Nup subcomplexes (Rout et al., 2000; Cronshaw et al., 2002; Alber et al., 2007a,b). The colocalization with *nup133Δ* NPC clusters might only reflect recruitment to a site with an increased density of defectively assembled NPCs that retain Rtn1 and Yop1. The insertion of RTNs and/or Yop1/DP1 in the outer leaflet of the pore membrane and localization of Pom–Nups to these membranes could be mutually exclusive sterically. Our future work will investigate whether RTN or Yop1/DP1 physically interacts with NPC components or whether they simply function to transiently maintain/induce membrane curvature during critical early steps of pore formation. In this latter model, subsequent incorporation of additional Nups–Poms would terminally stabilize pore structure and remove the need for the RTNs at mature NPCs.

Multiple members of the yNup84 subcomplex contain predicted amphipathic α-helix motifs implicated in sensing membrane curvature (Drin et al., 2007) or have structural homology to clathrin and coatomer protein I (COPI)/COPII vesicle coat proteins (Siniossoglou et al., 1996; Devos et al., 2004; Mans et al., 2004; Hsia et al., 2007). In vesicle budding, initiation of membrane curvature is promoted by accessory proteins that interact with the outer bilayer leaflet via amphiphatic α helices, α-solenoid, and

β-propeller motifs, and/or Bin–amphiphysin–Rvs (BAR) domains (Farsad and De Camilli, 2003; Stagg et al., 2007). Subsequent recruitment of the respective COP or clathrin coat proteins is thought to maintain the highly curved vesicle membrane. Thus, in a similar manner, the yNup84 and vNup107–160 subcomplex components are prime candidates for sustaining the mature NPC's curved pore membrane after the proposed initial RTN and/or Yop1/DP1 association with the pore. If RTNs and/or Yop1/DP1 is absent in mature NPCs, this could also facilitate NPC disassembly and allow for an unstable pore membrane to be rapidly resolved to an intact NE in interphase or during mitosis to ER tubules.

The formation of pores spanning the INM and ONM remains a poorly understood membrane fusion process. Collectively, our data strongly implicate RTNs and/or Yop1/DP1 as membrane proteins involved in nuclear pore formation and/or stability. The RTNs and Yop1/DP1 could function as underlying modulators of nuclear pore biogenesis, increasing assembly efficiency by stabilizing early pore assembly events and potentially coordinating the actions of Poms and the membrane-coating yNup84/vNup107–160 subcomplex. This work also highlights the overall dynamics of membrane systems in the cell and reveals further interconnections between the NE and tubular ER.

Materials and methods

Yeast strains, plasmids, genetics, and media

All strains and plasmids used in this study were generated as described in Tables S1 and S2 (available at http://www.jcb.org/cgi/content/full/jcb.200806174/DC1). In regard to strain construction, to integrate the gene for expression of the ER marker dsRed-HDEL, the plasmid (Bevis et al., 2002) was linearized with EcoRV and transformed into SWY3673 and SWY3677. To generate SWY201, a cassette containing the *HIS3* gene framed by 40 bases of sequence flanking the NUP120 locus was generated using pBM2815 as a template (gift of L. Riles, Washington University, St. Louis, MO), transformed, and integrated into diploid W303 cells. The resulting heterozygous diploid was sporulated and dissected to obtain viable haploid-null strains. Likewise, SWY4118 was generated by transformation and integration of a disruption cassette containing 40-bp flanking sequences homologous to the *SPO7* locus into SWY3811 covered by pSW3459. To generate SWY4124, a fragment containing *mCHERRY* framed by sequence immediately upstream and downstream of the *NIC96* stop codon was generated using pBS35 as a template (Shaner et al., 2004). Unless otherwise noted, all strains were grown at 23°C in YPD or synthetic minimal media lacking appropriate amino acids and supplemented with 2% dextrose. 5-FOA (US Biological) was used at a concentration of 1.0 mg/ml. Kanamycin resistance (conferred by the *KAN*^{R} gene) was selected on medium containing 200 µg/ml G418 (US Biological). All yeast genetic techniques were conducted according to standard procedures described previously (Sherman et al., 1986) with transformations by the lithium acetate method (Ito et al., 1983). References for published strains include Mortimer and Johnston (1986), Belanger et al. (1994), Wente and Blobel (1994), Wozniak et al. (1994), Aitchison et al. (1995), Gorsch et al. (1995), Goldstein et al. (1996), Kenna et al. (1996), Zabel et al. (1996), Bucci and Wente (1997, 1998), Emtage et al. (1997), Bailer et al. (1998), Ho et al. (1998), Winzeler et al. (1999), de Bruyn Kops and Guthrie (2001), Huh et al. (2003), Ryan et al. (2003), and Miao et al. (2006).

The plasmid pSW229 bearing *POM152* was constructed by subcloning a 5.19-kb fragment generated by PCR amplification from genomic DNA into the PstI site of pRS315 (Sikorski and Hieter, 1989). For pSW282, a 3.3-kb *NIC96* fragment was generated by PCR amplification from genomic DNA and was cloned into the BamHI site of pRS316 (Sikorski and Hieter, 1989). Likewise, pSW351 was generated by PCR amplification of a 4.6-kb *NUP133* genomic DNA fragment with oligonucleotide primers flanked with KpnI sites and was cloned into pRS316 to generate pSW351; a 2.2-kb *GLE2* gene fragment was PCR amplified using oligonucleotide primers flanked with XhoI and SacI sites and was cloned into pRS316 to generate pSW574; and a 4.6-kb *NUP120* fragment was PCR amplified with oligonucleotide primers flanked with BamHI sites and was cloned into pRS316 to generate pSW1079. The plasmid pSW3354 bearing *NUP85* was constructed by cloning the 4.12-kb *NUP85* gene fragment from pRAT9.15 (a gift from C. Cole, Dartmouth University, Lebanon, NH; Goldstein et al., 1996) into the SacI and XbaI sites of the *URA3/CEN* vector pRS316. A 2.5-kb *RTN1-GFP* fragment and a 1.8-kb *RTN1* fragment were PCR amplified from genomic DNA using oligonucleotides flanked by SpeI and SacI sites and were cloned into pRS315 and pRS316 to generate pSW3420 and pSW3459, respectively. The *rtn1-K48I* plasmids were generated by QuikChange XL Site-Directed Mutagenesis (Agilent Technologies) using pSW3420 as the PCR template. References for other published plasmids used include Belanger et al. (1994), Wente and Blobel (1994), Aitchison et al. (1995), Gorsch et al. (1995), Zabel et al. (1996), and Emtage et al. (1997).

Confocal microscopy

Strain SWY3747 and SWY4051 were grown in YPD at 23°C to an OD_{600} of 0.2 and were shifted to 34°C for 5 h. Localizations of GFP-tagged proteins and dsRed-HDEL were visualized by direct laser-scanning confocal microscopy. All images were taken on a confocal microscope (LSM 510; Carl Zeiss, Inc.) with a 63× Plan-Apochromat 1.4 NA oil immersion lens at a zoom of 3. GFP fluorescence was acquired using a 488-nm laser and a BP505–550-nm band pass filter, whereas dsRed fluorescence was acquired using a 543-nm laser and an LP560-nm long pass filter. Single-channel images were merged using ImageJ software (National Institutes of Health; Abramoff et al., 2004), and images were processed with ImageJ and Photoshop 9.0 (Adobe).

Biochemical fractionation

The *prp20-G282S* strain expressing Rtn1-GFP and GFP-Nic96 (SWY3748) was grown in 2-liter YPD cultures at 23°C to an OD_{600} of 0.2, divided, and either maintained at 23°C or shifted to 34°C for 5 h. Cell lysates were prepared as described previously (Ryan et al., 2003). Total lysate was centrifuged at 10,000 *g* for 10 min in a rotor (SLA-3000; Sorvall) to obtain the pellet and supernatant fractions. The high-speed membrane (HSM) fraction was sedimented by ultracentrifugation of the S fraction at 135,000 *g* for 1.5 h in a rotor (TLS-55; Beckman Coulter). Immunoblot analyses were performed with 1:1,000 anti-GFP, 1:1,000 anti-Pgk1 (mAb22C5; Invitrogen), or 1:25 anti-Nop1 (mAbD77; a gift from J. Aris, University of Florida, Gainesville, FL; Aris and Blobel, 1988).

Epifluorescence microscopy

Nuclear import assays were conducted as described in Strawn et al. (2004). The parental (BY4742) and *rtn1Δ yop1Δ* yeast strains (SWY3811) were grown at 23°C to early log phase and visualized. Direct epifluorescence and differential interference contrast images were acquired using a microscope (BX50; Olympus) with a UPlanF1 100× NA 1.30 oil immersion objective and camera (CoolSNAP HQ; Photometrics). Images were collected and scaled equivalently using MetaVue version 4.6 (MDS Analytical Technologies) or ImagePro Express (Media Cybernetics) and processed with Photoshop 9.0 software.

For indirect immunofluorescence, cells were fixed in 3.7% formaldehyde and 10% methanol for 10 min and processed as previously described (Strawn et al., 2004). Samples were incubated for 16 h at 4°C with affinity-purified rabbit polyclonal anti-Nup116C (1:50), affinity-purified rabbit polyclonal anti-GLFG (1:800), affinity-purified rabbit polyclonal anti-GFP (1:250), or mAb414 (1:2 tissue culture supernatant; Davis and Blobel, 1986) antibodies. Bound antibodies were detected by incubation with Alexa Fluor 488–conjugated goat anti–rabbit IgG (1:300; Jackson ImmunoResearch Laboratories) or Alexa Fluor 594–conjugated goat anti–mouse IgG (1:400). DNA was stained with 0.1 µg/ml DAPI, and samples were mounted for imaging in 90% glycerol and 1 mg/ml *p*-phenylenediamine (Sigma-Aldrich), pH 8.0. Images were collected as described for direct epifluorescence imaging.

Thin-section EM

Parental (BY4724) and *rtn1Δ yop1Δ* yeast strains (SWY3811) were grown in YPD at 23°C to early log phase and processed to preserve protein and membrane structures as previously described (Wente and Blobel, 1993). Ultra-thin sections (50–60 nm) of the embedded samples were cut on an ultramicrotome (Ultracut UCT 54; Leica) and collected on formvar-coated nickel grids stabilized with carbon (Electron Microscopy Sciences). Grids were contrasted with uranyl acetate and lead citrate and examined on a transmission electron microscope (CM12; Philips) equipped with a 2-megapixel charge-coupled device camera (MegaPlus ES 4.0; Advanced Microscopy Techniques).

Depletion of *Xenopus* WGA-binding proteins

Biotinylated WGA (Biomeda) was immobilized under saturating conditions on streptavidin-coated magnetic beads (Invitrogen). After excessive washing,

beads were incubated with freshly prepared cytosol (membrane free; Walther et al., 2003a,b) rotating on ice for 30 min. Depleted cytosol was immediately snap frozen and stored in liquid nitrogen. Depletion of Nups was verified by Western blotting using mAb414 antibody (Millipore).

Xenopus in vitro assembly assays

Xenopus egg extracts and sperm chromatin were prepared as previously described (D'Angelo et al., 2006). Membranes were stained with $DiIC_{16}(3)$ as previously described (Hetzer et al., 2000). Nuclei were formed by either the classical method of combining fragmented ER membranes, cytosol, and sperm chromatin on ice or by first reconstituting the ER network by mixing membranes with cytosol and incubating at room temperature for 10–20 min and carefully adding sperm chromatin to the intact ER network. ER was assembled with *Xenopus* egg extracts as previously described (Anderson and Hetzer, 2007). Intact ER network was pipetted with cutoff tips to reduce fragmentation. Dextran exclusion assays were performed as described previously (D'Angelo et al., 2006) with the following modifications to more efficiently block diffusion of fluorescently labeled 70-kD dextrans (Invitrogen and Sigma-Aldrich) through NPCs. We incubated assembled nuclei with a mixture of 10 µg/ml biotinylated WGA and 10 µg/ml streptavidin for 20 min before the addition of dextrans, which form a high-molecular plug at the pores.

Online supplemental material

Fig. S1 shows the localization of Yop1-GFP and Sec63-GFP in *prp20-G282S* cells. Fig. S2 shows further analysis of *rtn1Δ yop1Δ* genetic analysis with *nup* and *pom* mutants, including *nup/pom* parental strains. Fig. S3 illustrates the rescue of NPC clustering with *rtn1-K48I* expression in *rtn1Δ yop1Δ GFP-nic96* cells. Fig. S4 shows *Xenopus* in vitro assembly assays. Table S1 lists all of the yeast strains used in this study. Table S2 details all of the plasmids used. Online supplemental material is available at http://www.jcb.org/cgi/content/full/jcb.200806174/DC1.

We thank J. Aitchison, J. Aris, K. Belanger, M. Bucci, C. Cole, D. Goldfarb, C. Guthrie, E. Hurt, G. Voeltz, and R. Wozniak for reagents and members of the Wente and Hetzer laboratories for critical discussions. EM was performed by Magnify, Inc.

This work was supported by a grant from the National Institutes of Health (RO1 GM57438 to M.W. Hetzer and S.R. Wente). Confocal microscopy was performed with the Vanderbilt University Medical Center Cell Imaging Shared Resource (supported by National Institutes of Health grants CA68485, DK20593, DK58404, HD15052, DK59637, and EY08126).

Submitted: 30 June 2008
Accepted: 6 February 2009

References

Abramoff, M., P. Magelhaes, and S. Ram. 2004. Image processing with ImageJ. *Biophotonics International*. 11:36–42.

Aitchison, J.D., M.P. Rout, M. Marelli, G. Blobel, and R.W. Wozniak. 1995. Two novel related yeast nucleoporins Nup170p and Nup157p: complementation with the vertebrate homologue Nup155p and functional interactions with the yeast nuclear pore-membrane protein Pom152p. *J. Cell Biol.* 131:1133–1148.

Alber, F., S. Dokudovskaya, L.M. Veenhoff, W. Zhang, J. Kipper, D. Devos, A. Suprapto, O. Karni-Schmidt, R. Williams, B.T. Chait, et al. 2007a. Determining the architectures of macromolecular assemblies. *Nature*. 450:683–694.

Alber, F., S. Dokudovskaya, L.M. Veenhoff, W. Zhang, J. Kipper, D. Devos, A. Suprapto, O. Karni-Schmidt, R. Williams, B.T. Chait, et al. 2007b. The molecular architecture of the nuclear pore complex. *Nature*. 450:695–701.

Anderson, D.J., and M.W. Hetzer. 2007. Nuclear envelope formation by chromatin-mediated reorganization of the endoplasmic reticulum. *Nat. Cell Biol.* 9:1160–1166.

Anderson, D.J., and M.W. Hetzer. 2008. Reshaping of the endoplasmic reticulum limits the rate for nuclear envelope formation. *J. Cell Biol.* 182:911–924.

Antonin, W., C. Franz, U. Haselmann, C. Antony, and I.W. Mattaj. 2005. The integral membrane nucleoporin pom121 functionally links nuclear pore complex assembly and nuclear envelope formation. *Mol. Cell*. 17:83–92.

Antonin, W., J. Ellenberg, and E. Dultz. 2008. Nuclear pore complex assembly through the cell cycle: regulation and membrane organization. *FEBS Lett.* 582:2004–2016.

Aris, J.P., and G. Blobel. 1988. Identification and characterization of a yeast nucleolar protein that is similar to a rat liver nucleolar protein. *J. Cell Biol.* 107:17–31.

Audhya, A., A. Desai, and K. Oegema. 2007. A role for Rab5 in structuring the endoplasmic reticulum. *J. Cell Biol.* 178:43–56.

Bailer, S.M., S. Siniossoglou, A. Podtelejnikov, A. Hellwig, M. Mann, and E.C. Hurt. 1998. Nup116p and Nup100p are interchangeable through a conserved motif which constitutes a docking site for the mRNA export factor Gle2p. *EMBO J.* 17:1107–1119.

Baker, K.E., J. Coller, and R. Parker. 2004. The yeast Apq12 protein affects nucleocytoplasmic mRNA transport. *RNA*. 10:1352–1358.

Belanger, K.D., M.A. Kenna, S. Wei, and L.I. Davis. 1994. Genetic and physical interactions between Srp1p and nuclear pore complex proteins Nup1p and Nup2p. *J. Cell Biol.* 126:619–630.

Berke, I.C., T. Boehmer, G. Blobel, and T.U. Schwartz. 2004. Structural and functional analysis of Nup133 domains reveals modular building blocks of the nuclear pore complex. *J. Cell Biol.* 167:591–597.

Bevis, B.J., A.T. Hammond, C.A. Reinke, and B.S. Glick. 2002. De novo formation of transitional ER sites and Golgi structures in *Pichia pastoris*. *Nat. Cell Biol.* 4:750–756.

Bucci, M., and S.R. Wente. 1997. In vivo dynamics of nuclear pore complexes in yeast. *J. Cell Biol.* 136:1185–1199.

Bucci, M., and S.R. Wente. 1998. A novel fluorescence-based genetic strategy identifies mutants of *Saccharomyces cerevisiae* defective for nuclear pore complex assembly. *Mol. Biol. Cell*. 9:2439–2461.

Campbell, J.L., A. Lorenz, K.L. Witkin, T. Hays, J. Loidl, and O. Cohen-Fix. 2006. Yeast nuclear envelope subdomains with distinct abilities to resist membrane expansion. *Mol. Biol. Cell*. 17:1768–1778.

Chial, H.J., M.P. Rout, T.H. Giddings, and M. Winey. 1998. *Saccharomyces cerevisiae* Ndc1p is a shared component of nuclear pore complexes and spindle pole bodies. *J. Cell Biol.* 143:1789–1800.

Cronshaw, J.M., A.N. Krutchinsky, W. Zhang, B.T. Chait, and M.J. Matunis. 2002. Proteomic analysis of the mammalian nuclear pore complex. *J. Cell Biol.* 158:915–927.

D'Angelo, M.A., D.J. Anderson, E. Richard, and M.W. Hetzer. 2006. Nuclear pores form de novo from both sides of the nuclear envelope. *Science*. 312:440–443.

Davis, L.I., and G. Blobel. 1986. Identification and characterization of a nuclear pore complex protein. *Cell*. 45:699–709.

de Bruyn Kops, A., and C. Guthrie. 2001. An essential nuclear envelope integral membrane protein, Brr6p, required for nuclear transport. *EMBO J.* 20:4183–4193.

De Craene, J.O., J. Coleman, P. Estrada de Martin, M. Pypaert, S. Anderson, J.R. Yates III, S. Ferro-Novick, and P. Novick. 2006. Rtn1p is involved in structuring the cortical endoplasmic reticulum. *Mol. Biol. Cell*. 17:3009–3020.

Devos, D., S. Dokudovskaya, F. Alber, R. Williams, B.T. Chait, A. Sali, and M.P. Rout. 2004. Components of coated vesicles and nuclear pore complexes share a common molecular architecture. *PLoS Biol.* 2:e380.

Doye, V., and E. Hurt. 1997. From nucleoporins to nuclear pore complexes. *Curr. Opin. Cell Biol.* 9:401–411.

Drin, G., J.F. Casella, R. Gautier, T. Boehmer, T.U. Schwartz, and B. Antonny. 2007. A general amphipathic alpha-helical motif for sensing membrane curvature. *Nat. Struct. Mol. Biol.* 14:138–146.

Dultz, E., E. Zanin, C. Wurzenberger, M. Braun, G. Rabut, L. Sironi, and J. Ellenberg. 2008. Systematic kinetic analysis of mitotic dis- and reassembly of the nuclear pore in living cells. *J. Cell Biol.* 180:857–865.

Emtage, J.L., M. Bucci, J.L. Watkins, and S.R. Wente. 1997. Defining the essential functional regions of the nucleoporin Nup145p. *J. Cell Sci.* 110:911–925.

Farsad, K., and P. De Camilli. 2003. Mechanisms of membrane deformation. *Curr. Opin. Cell Biol.* 15:372–381.

Finlay, D.R., and D.J. Forbes. 1990. Reconstitution of biochemically altered nuclear pores: transport can be eliminated and restored. *Cell*. 60:17–29.

Geng, J., M.E. Shin, P.M. Gilbert, R.N. Collins, and C.G. Burd. 2005. *Saccharomyces cerevisiae* Rab-GDI displacement factor ortholog Yip3p forms distinct complexes with the Ypt1 Rab GTPase and the reticulon Rtn1p. *Eukaryot. Cell*. 4:1166–1174.

Goldstein, A.L., C.A. Snay, C.V. Heath, and C.N. Cole. 1996. Pleiotropic nuclear defects associated with a conditional allele of the novel nucleoporin Rat9p/Nup85p. *Mol. Biol. Cell*. 7:917–934.

Gorsch, L.C., T.C. Dockendorff, and C.N. Cole. 1995. A conditional allele of the novel repeat-containing yeast nucleoporin RAT7/NUP159 causes both rapid cessation of mRNA export and reversible clustering of nuclear pore complexes. *J. Cell Biol.* 129:939–955.

Greber, U.F., A. Senior, and L. Gerace. 1990. A major glycoprotein of the nuclear pore complex is a membrane-spanning polypeptide with a large lumenal domain and a small cytoplasmic tail. *EMBO J.* 9:1495–1502.

Hallberg, E., R.W. Wozniak, and G. Blobel. 1993. An integral membrane protein of the pore membrane domain of the nuclear envelope contains a nucleoporin-like region. *J. Cell Biol.* 122:513–521.

Harel, A., R.C. Chan, A. Lachish-Zalait, E. Zimmerman, M. Elbaum, and D.J. Forbes. 2003a. Importin {beta} negatively regulates nuclear membrane fusion and nuclear pore complex assembly. *Mol. Biol. Cell*. 14:4387–4396.

Harel, A., A.V. Orjalo, T. Vincent, A. Lachish-Zalait, S. Vasu, S. Shah, E. Zimmerman, M. Elbaum, and D.J. Forbes. 2003b. Removal of a single pore subcomplex results in vertebrate nuclei devoid of nuclear pores. *Mol. Cell*. 11:853–864.

Hetzer, M., D. Bilbao-Cortes, T.C. Walther, O.J. Gruss, and I.W. Mattaj. 2000. GTP hydrolysis by Ran is required for nuclear envelope assembly. *Mol. Cell*. 5:1013–1024.

Hetzer, M.W., T.C. Walther, and I.W. Mattaj. 2005. Pushing the envelope: structure, function, and dynamics of the nuclear periphery. *Annu. Rev. Cell Dev. Biol.* 21:347–380.

Ho, A.K., G.A. Raczniak, E.B. Ives, and S.R. Wente. 1998. The integral membrane protein Snl1p is genetically linked to yeast nuclear pore complex function. *Mol. Biol. Cell*. 9:355–373.

Hsia, K.C., P. Stavropoulos, G. Blobel, and A. Hoelz. 2007. Architecture of a coat for the nuclear pore membrane. *Cell*. 131:1313–1326.

Hu, J., Y. Shibata, C. Voss, T. Shemesh, Z. Li, M. Coughlin, M.M. Kozlov, T.A. Rapoport, and W.A. Prinz. 2008. Membrane proteins of the endoplasmic reticulum induce high-curvature tubules. *Science*. 319:1247–1250.

Huh, W.K., J.V. Falvo, L.C. Gerke, A.S. Carroll, R.W. Howson, J.S. Weissman, and E.K. O'Shea. 2003. Global analysis of protein localization in budding yeast. *Nature*. 425:686–691.

Ito, H., Y. Fukuda, K. Murata, and A. Kimura. 1983. Transformation of intact yeast cells treated with alkali cations. *J. Bacteriol.* 153:163–168.

Kenna, M.A., J.G. Petranka, J.L. Reilly, and L.I. Davis. 1996. Yeast Nle3p/Nup170p is required for normal stoichiometry of FG nucleoporins within the nuclear pore complex. *Mol. Cell. Biol.* 16:2025–2036.

Kiseleva, E., K.N. Morozova, G.K. Voeltz, T.D. Allen, and M.W. Goldberg. 2007. Reticulon 4a/NogoA locates to regions of high membrane curvature and may have a role in nuclear envelope growth. *J. Struct. Biol.* 160:224–235.

Lau, C.K., T.H. Giddings Jr., and M. Winey. 2004. A novel allele of *Saccharomyces cerevisiae NDC1* reveals a potential role for the spindle pole body component Ndc1p in nuclear pore assembly. *Eukaryot. Cell*. 3:447–458.

Lewis, A., R. Felberbaum, and M. Hochstrasser. 2007. A nuclear envelope protein linking nuclear pore basket assembly, SUMO protease regulation, and mRNA surveillance. *J. Cell Biol.* 178:813–827.

Li, O., C.V. Heath, D.C. Amberg, T.C. Dockendorff, C.S. Copeland, M. Snyder, and C.N. Cole. 1995. Mutation or deletion of the *Saccharomyces cerevisiae RAT3/NUP133* gene causes temperature-dependent nuclear accumulation of poly(A)+ RNA and constitutive clustering of nuclear pore complexes. *Mol. Biol. Cell*. 6:401–417.

Lim, R.Y., U. Aebi, and B. Fahrenkrog. 2008. Towards reconciling structure and function in the nuclear pore complex. *Histochem. Cell Biol.* 129:105–116.

Liu, Q., N. Pante, T. Misteli, M. Elsagga, M. Crisp, D. Hodzic, B. Burke, and K.J. Roux. 2007. Functional association of Sun1 with nuclear pore complexes. *J. Cell Biol.* 178:785–798.

Lutzmann, M., R. Kunze, A. Buerer, U. Aebi, and E. Hurt. 2002. Modular self-assembly of a Y-shaped multiprotein complex from seven nucleoporins. *EMBO J.* 21:387–397.

Macaulay, C., and D.J. Forbes. 1996. Assembly of the nuclear pore: biochemically distinct steps revealed with NEM, GTP gamma S, and BAPTA. *J. Cell Biol.* 132:5–20.

Madrid, A.S., J. Mancuso, W.Z. Cande, and K. Weis. 2006. The role of the integral membrane nucleoporins Ndc1p and Pom152p in nuclear pore complex assembly and function. *J. Cell Biol.* 173:361–371.

Mans, B.J., V. Anantharaman, L. Aravind, and E.V. Koonin. 2004. Comparative genomics, evolution and origins of the nuclear envelope and nuclear pore complex. *Cell Cycle*. 3:1612–1637.

Mansfeld, J., S. Guttinger, L.A. Hawryluk-Gara, N. Pante, M. Mall, V. Galy, U. Haselmann, P. Muhlhausser, R.W. Wozniak, I.W. Mattaj, et al. 2006. The conserved transmembrane nucleoporin NDC1 is required for nuclear pore complex assembly in vertebrate cells. *Mol. Cell*. 22:93–103.

Marelli, M., J.D. Aitchison, and R.W. Wozniak. 1998. Specific binding of the karyopherin Kap121p to a subunit of the nuclear pore complex containing Nup53p, Nup59p, and Nup170p. *J. Cell Biol.* 143:1813–1830.

Maul, G.G., J.W. Price, and M.W. Lieberman. 1971. Formation and distribution of nuclear pore complexes in interphase. *J. Cell Biol.* 51:405–418.

Miao, M., K.J. Ryan, and S.R. Wente. 2006. The integral membrane protein Pom34p functionally links nucleoporin subcomplexes. *Genetics*. 172:1441–1457.

Miller, J.P., R.S. Lo, A. Ben-Hur, C. Desmarais, I. Stagljar, W.S. Noble, and S. Fields. 2005. Large-scale identification of yeast integral membrane protein interactions. *Proc. Natl. Acad. Sci. USA*. 102:12123–12128.

Miller, M.W., and J.A. Hanover. 1994. Functional nuclear pores reconstituted with beta 1-4 galactose-modified O-linked N-acetylglucosamine glycoproteins. *J. Biol. Chem.* 269:9289–9297.

Mortimer, R.K., and J.R. Johnston. 1986. Genealogy of principal strains of the yeast genetic stock center. *Genetics*. 113:35–43.

Nehrbass, U., M.P. Rout, S. Maguire, G. Blobel, and R.W. Wozniak. 1996. The yeast nucleoporin Nup188p interacts genetically and physically with the core structures of the nuclear pore complex. *J. Cell Biol.* 133:1153–1162.

Oertle, T., M. Klinger, C.A. Stuermer, and M.E. Schwab. 2003. A reticular rhapsody: phylogenic evolution and nomenclature of the RTN/Nogo gene family. *FASEB J.* 17:1238–1247.

Rout, M.P., J.D. Aitchison, A. Suprapto, K. Hjertaas, Y. Zhao, and B.T. Chait. 2000. The yeast nuclear pore complex: composition, architecture, and transport mechanism. *J. Cell Biol.* 148:635–651.

Ryan, K.J., J.M. McCaffery, and S.R. Wente. 2003. The Ran GTPase cycle is required for yeast nuclear pore complex assembly. *J. Cell Biol.* 160:1041–1053.

Ryan, K.J., Y. Zhou, and S.R. Wente. 2007. The karyopherin Kap95 regulates nuclear pore complex assembly into intact nuclear envelopes in vivo. *Mol. Biol. Cell*. 18:886–898.

Santos-Rosa, H., J. Leung, N. Grimsey, S. Peak-Chew, and S. Siniossoglou. 2005. The yeast lipin Smp2 couples phospholipid biosynthesis to nuclear membrane growth. *EMBO J.* 24:1931–1941.

Scarcelli, J.J., C.A. Hodge, and C.N. Cole. 2007. The yeast integral membrane protein Apq12 potentially links membrane dynamics to assembly of nuclear pore complexes. *J. Cell Biol.* 178:799–812.

Schneiter, R., M. Hitomi, A.S. Ivessa, E.V. Fasch, S.D. Kohlwein, and A.M. Tartakoff. 1996. A yeast acetyl coenzyme A carboxylase mutant links very-long-chain fatty acid synthesis to the structure and function of the nuclear membrane-pore complex. *Mol. Cell. Biol.* 16:7161–7172.

Shaner, N.C., R.E. Campbell, P.A. Steinbach, B.N. Giepmans, A.E. Palmer, and R.Y. Tsein. 2004. Improved monomeric red, orange and yellow fluorescent proteins derived from *Discosoma* sp. red fluorescent protein. *Nat. Biotechnol.* 22:1567–1572.

Sheetz, M.P., R.G. Painter, and S.J. Singer. 1976. Biological membranes as bilayer couples. III. Compensatory shape changes induced in membranes. *J. Cell Biol.* 70:193–203.

Sherman, F., G.R. Fink, and J.B. Hicks. 1986. Methods in Yeast Genetics: Laboratory Course Manual for Methods in Genetics. Cold Spring Harbor Laboratory, Cold Spring Harbor, NY. 186 pp.

Shibata, Y., C. Voss, J.M. Rist, J. Hu, T.A. Rapoport, W.A. Prinz, and G.K. Voeltz. 2008. The reticulon and DP1/Yop1p proteins form immobile oligomers in the tubular endoplasmic reticulum. *J. Biol. Chem.* 283:18892–18904.

Shulga, N., P. Roberts, Z. Gu, L. Spitz, M.M. Tabb, M. Nomura, and D.S. Goldfarb. 1996. In vivo nuclear transport kinetics in *Saccharomyces cerevisiae*: a role for heat shock protein 70 during targeting and translocation. *J. Cell Biol.* 135:329–339.

Shulga, N., N. Mosammaparast, R. Wozniak, and D.S. Goldfarb. 2000. Yeast nucleoporins involved in passive nuclear envelope permeability. *J. Cell Biol.* 149:1027–1038.

Sikorski, R.S., and P. Hieter. 1989. A system of shuttle vectors and yeast host strains designed for efficient manipulation of DNA in *Saccharomyces cerevisiae*. *Genetics*. 122:19–27.

Siniossoglou, S., C. Wimmer, M. Rieger, V. Doye, H. Tekotte, C. Weise, S. Emig, A. Segref, and E.C. Hurt. 1996. A novel complex of nucleoporins, which includes Sec13p and a Sec13p homolog, is essential for normal nuclear pores. *Cell*. 84:265–275.

Siniossoglou, S., H. Santos-Rosa, J. Rappsilber, M. Mann, and E. Hurt. 1998. A novel complex of membrane proteins required for formation of a spherical nucleus. *EMBO J.* 17:6449–6464.

Siniossoglou, S., M. Lutzmann, H. Santos-Rosas, K. Leonard, S. Mueller, U. Aebi, and E. Hurt. 2000. Structure and assembly of the Nup84p complex. *J. Cell Biol.* 149:41–54.

Sondermann, H., A.K. Ho, L.L. Listenberger, K. Siegers, I. Moarefi, S.R. Wente, F.-U. Hartl, and J.C. Young. 2002. Prediction of novel Bag-1 homologs based on structure/function analysis identifies Snl1p as an Hsp70 co-chaperone in *Saccharomyces cerevisiae*. *J. Biol. Chem.* 277:33220–33227.

Stagg, S.M., P. LaPointe, and W.E. Balch. 2007. Structural design of cage and coat scaffolds that direct membrane traffic. *Curr. Opin. Struct. Biol.* 17:221–228.

Stavru, F., B.B. Hulsmann, A. Spang, E. Hartmann, V.C. Cordes, and D. Gorlich. 2006. NDC1: a crucial membrane-integral nucleoporin of metazoan nuclear pore complexes. *J. Cell Biol.* 173:509–519.

Strawn, L.A., T. Shen, N. Shulga, D.S. Goldfarb, and S.R. Wente. 2004. Minimal nuclear pore complexes define FG repeat domains essential for transport. *Nat. Cell Biol.* 6:197–206.

Terry, L.J., and S.R. Wente. 2007. Nuclear mRNA export requires specific FG nucleoporins for translocation through the nuclear pore complex. *J. Cell Biol.* 178:1121–1132.

Terry, L.J., E.B. Shows, and S.R. Wente. 2007. Crossing the nuclear envelope: hierarchical regulation of nucleocytoplasmic transport. *Science*. 318:1412–1416.

Timney, B.L., J. Tetenbaum-Novatt, D.S. Agate, R. Williams, W. Zhang, B.T. Chait, and M.P. Rout. 2006. Simple kinetic relationships and nonspecific competition govern nuclear import rates in vivo. *J. Cell Biol.* 175:579–593.

Voeltz, G.K., W.A. Prinz, Y. Shibata, J.M. Rist, and T.A. Rapoport. 2006. A class of membrane proteins shaping the tubular endoplasmic reticulum. *Cell*. 124:573–586.

Walther, T.C., A. Alves, H. Pickersgill, I. Loiodice, M. Hetzer, V. Galy, B.B. Hulsmann, T. Kocher, M. Wilm, T. Allen, et al. 2003a. The conserved Nup107-160 complex is critical for nuclear pore complex assembly. *Cell*. 113:195–206.

Walther, T.C., P. Askjaer, M. Gentzel, A. Habermann, G. Griffiths, M. Wilm, I.W. Mattaj, and M. Hetzer. 2003b. RanGTP mediates nuclear pore complex assembly. *Nature*. 424:689–694.

Wente, S.R., and G. Blobel. 1993. A temperature-sensitive NUP116 null mutant forms a nuclear envelope seal over the yeast nuclear pore complex thereby blocking nucleocytoplasmic traffic. *J. Cell Biol.* 123:275–284.

Wente, S.R., and G. Blobel. 1994. NUP145 encodes a novel yeast glycine-leucine-phenylalanine-glycine (GLFG) nucleoporin required for nuclear envelope structure. *J. Cell Biol.* 125:955–969.

Winey, M., D. Yarar, T.H. Giddings Jr., and D.N. Mastronarde. 1997. Nuclear pore complex number and distribution throughout the *Saccharomyces cerevisiae* cell cycle by three-dimensional reconstruction from electron micrographs of nuclear envelopes. *Mol. Biol. Cell*. 8:2119–2132.

Winzeler, E.A., D.D. Shoemaker, A. Astromoff, H. Liang, K. Anderson, B. Andre, R. Bangham, R. Benito, J.D. Boeke, H. Bussey, et al. 1999. Functional characterization of the *S. cerevisiae* genome by gene deletion and parallel analysis. *Science*. 285:901–906.

Wozniak, R.W., G. Blobel, and M.P. Rout. 1994. POM152 is an integral protein of the pore membrane domain of the yeast nuclear envelope. *J. Cell Biol.* 125:31–42.

Zabel, U., D. Doye, H. Tekotte, R. Wepf, P. Grandi, and E.C. Hurt. 1996. Nic96p is required for nuclear pore formation and functionally interacts with a novel nucleoporin, Nup188p. *J. Cell Biol.* 133:1141–1152.